SCIENCE CHINA
Earth Sciences

•REVIEW•

May 2021 Vol.64 No.5: 691–715
https://doi.org/10.1007/s11430-020-9735-5

Geological settings and metallogenesis of high-grade iron deposits in China

Zhaochong ZHANG[1*], Houmin LI[2], Jianwei LI[3], Xie-Yan SONG[4], Hao HU[3], Lixing LI[2], Fengmei CHAI[5], Tong HOU[1] & Deru XU[6,7]

[1] *State Key Laboratory of Geological Processes and Mineral Resources, China University of Geosciences, Beijing 100083, China;*
[2] *Institute of Mineral Resources, Chinese Academy of Geological Sciences, Beijing 100037, China;*
[3] *State Key Laboratory of Geological Processes and Mineral Resources, China University of Geosciences, Wuhan 430074, China;*
[4] *State Key Laboratory of Ore Deposit Geochemistry, Institute of Geochemistry, Chinese Academy of Sciences, Guiyang 550002, China;*
[5] *Xinjiang Key Laboratory for Geodynamic Processes and Metallogenic Prognosis of the Central Asian Orogenic Belt, Xinjiang University, Urumqi 830046, China;*
[6] *State Key Laboratory of Nuclear Resources and Environment, East China University of Technology, Nanchang 330013, China;*
[7] *CAS Key Laboratory of Mineralogy and Metallogeny, Guangzhou Institute of Geochemistry, Chinese Academy of Sciences, Guangzhou 510640, China*

Received July 14, 2020; revised January 7, 2021; accepted February 1, 2021; published online April 7, 2021

Abstract The predominant types of high-grade iron deposits in China include skarn, sedimentary metamorphic (banded iron-formation, BIF-type), continental/submarine volcanic-hosted and magmatic Fe-Ti-V oxide deposits. Based on a comprehensive review of current studies on these deposits, this paper suggests that the oxygen concentration in atmosphere played an important role for the formation of BIFs, whereas the tectonic setting and deep magmatic differentiation processes are more important for the other types. Notably, both high temperature and high pressure experiments and melt inclusion studies indicate that during the differentiation, high temperature magmas could develop iron-rich magma via liquid immiscibility but not pure oxide melt ("iron ore magma"). Fe-P melt could be generated directly by liquid immiscibility under hydrous and oxidized condition. The formation of high-grade iron deposits is mostly associated with the processes related to multiple stages of superimposition, e.g., desilicionization and iron enrichment, removal of impurity, and remobilization and re-precipitation of iron. According to the temporal evolution, the high-grade iron deposit could be divided into multi-episode superimposition type (temporally discontinuous mineralization) and multi-stage superimposition type (temporally continuous mineralization). The former is represented by the sedimentary metamorphic iron deposit, and the latter includes those related to magmatic-hydrothermal fluids (e.g., skarn, volcanic-hosted and magmatic types).

Keywords High-grade iron deposit, Metallogenesis, Iron ore magma, Liquid immiscibility, Fe-rich fluid

Citation: Zhang Z, Li H, Li J, Song X Y, Hu H, Li L, Chai F, Hou T, Xu D. 2021. Geological settings and metallogenesis of high-grade iron deposits in China. Science China Earth Sciences, 64(5): 691–715, https://doi.org/10.1007/s11430-020-9735-5

1. Introduction

Although China has a rich reserve of iron ores, high-grade iron ores (>50 wt.% Fe) have been scare, with average grade only about 30 wt.% Fe (Figure 1a). Globally, more than 85% of iron ores, especially high-grade iron ore reserves are from banded iron-formation (BIF)-type iron deposit (Hagemann et al., 2016). Most giant BIF-type high-grade iron deposits had exclusively developed in stable cratons (e.g., Morris, 1983), and after precipitation of BIFs in sea water, subsequent

*Corresponding author (email: zczhang@cugb.edu.cn)

weathering and leaching are required to generate the high-grade hematite deposits. During the 20th century, extensive exploration and genesis research of BIF-type iron deposits in China were carried out, targeting for such weathering-leaching BIF-type deposits, but the results were quite unsatisfying (Yao, 1993). The studies at the time and afterwards revealed that extensive and strong tectonic-magmatic activities had developed in China after Proterozoic era and hence neither pristine BIF nor subsequent high-grade weathering-leaching BIF-type iron deposits could be produced or preserved. However, the strong and extensive tectonic-magmatic activities rather provided a favorable condition for the formation of high-grade iron deposits associated with magmatism, including skarn, volcanic-hosted and magmatic types and enrichment related to superimposition and reworking of the sedimentary metamorphic types (Li J W et al., 2019).

Many case studies have mentioned that the formation of high-grade iron deposits could be genetically associated with the two key processes as stated above, i.e., multi-stage superimposition and reworking, and direct injection of iron ore magma (Li J W et al., 2019). Nevertheless, the mechanism by which high-grade iron ores produced, the key controlling factors for diverse high-grade ore genesis, and whether iron ore magmas exist are still quite controversial. Thus, in order to improve our understanding on and elucidate the formation of high-grade iron deposits in China, this paper, based on comprehensive reviews on previous studies, shed new lights on some of the relevant key scientific issues.

2. High-grade iron ore resources in China

Based on the relationship between iron ore and their structure and host rock-types, Dill (2010) classified all the iron deposits into four major types: (1) magmatic iron deposits, (2) structure-related iron deposits, (3) sedimentary iron deposits and (4) metamorphic iron deposits. In contrast, due to their complexity, Chinese iron deposits had been classified into eight major types by Zhao et al. (2004), including magmatic, skarn, volcanic-hosted, hydrothermal, sedimentary metamorphic, sedimentary, weather-leach and unidentified types. Therein, the volcanic-hosted type has been further divided into continental- and submarine-volcanic types. Continental volcanic iron deposit is also known as "porphyry iron deposits" (VIDRGMLCJV, 1977), and internationally, it is known as Kiruna-type or Iron Oxide-Apatite deposits (i.e., IOA type; Nyström and Henriquez, 1994; Hou et al., 2018). For magmatic iron deposits, they could be further divided into Panzhihua- and Damiao-types, which are hosted in layered intrusions and Proterozoic anorthosite massif, respectively. By comparison, Zhang et al. (2014b) pointed out that most of the Chinese high-grade iron deposits could be comparable within the two classification systems, i.e., Dill (2010) and Zhao et al. (2004). This paper uses the classification of Zhao et al. (2004). The hydrothermal and unidentified types in China are economically unimportant, thus will not be discussed further in this paper.

Statistics diagrams in Figure 1b, 1c show most of the large-scale iron deposits in China belong to the sedimentary metamorphic type, which is thus the largest reserves of domestic iron reserve. This feature, i.e., iron reserve dominated by BIF-related iron ores, is consistent with those in other parts of the world. However, in terms of high-grade iron ores, the most important type in China is skarn, which account for >50% of the reserve of the high-grade ores, followed by sedimentary metamorphic, volcanic-hosted, sedimentary type and magmatic type (Figure 1d). Such a feature in high-grade iron ores is indeed distinct from those worldwide, which are mainly sedimentary metamorphic hematite type (weathering-leaching) ores. However, among these Chinese high-grade iron deposits, the ores from sedimentary type iron deposits are largely unavailable due to its refractory nature, and thus economically insignificant. In contrast, although the proportion of high-grade iron ore in magmatic iron deposits is relatively low, they are vanadium-titanium magnetite ores which are very important for industry. Therefore, the main types of high-grade iron deposits in China include four types, i.e., sedimentary metamorphic, skarn, volcanic-hosted and magmatic types.

3. Spatio-temporal distribution and metallogenic geological settings of the iron deposits in China

The types of iron deposits show its distinct time-dependence characteristics as their formation are both temporally and spatially related to major geological events. For instance, sedimentary metamorphic iron deposits were those that were formed initially by BIFs which had experienced subsequent metamorphism. It is well known that BIFs are generally deposited during Archean and Paleoproterozoic eras, and are closely related to submarine volcanic hydrothermal activities and the global Great Oxidation Event (GOE; e.g., Isley, 1995). In addition, the Neoproterozoic "Snowball Earth" event had also formed BIFs. Except sedimentary metamorphic iron deposits, the other types of iron deposits were also formed in various tectonic settings or events since Proterozoic era (Figure 2).

3.1 Geological settings of different iron deposit types

3.1.1 Geological setting of sedimentary metamorphic iron deposits

The BIFs are iron-rich (Fe>15 wt.%) Precambrian chemical sedimentary rocks and composed of banded quartz and iron

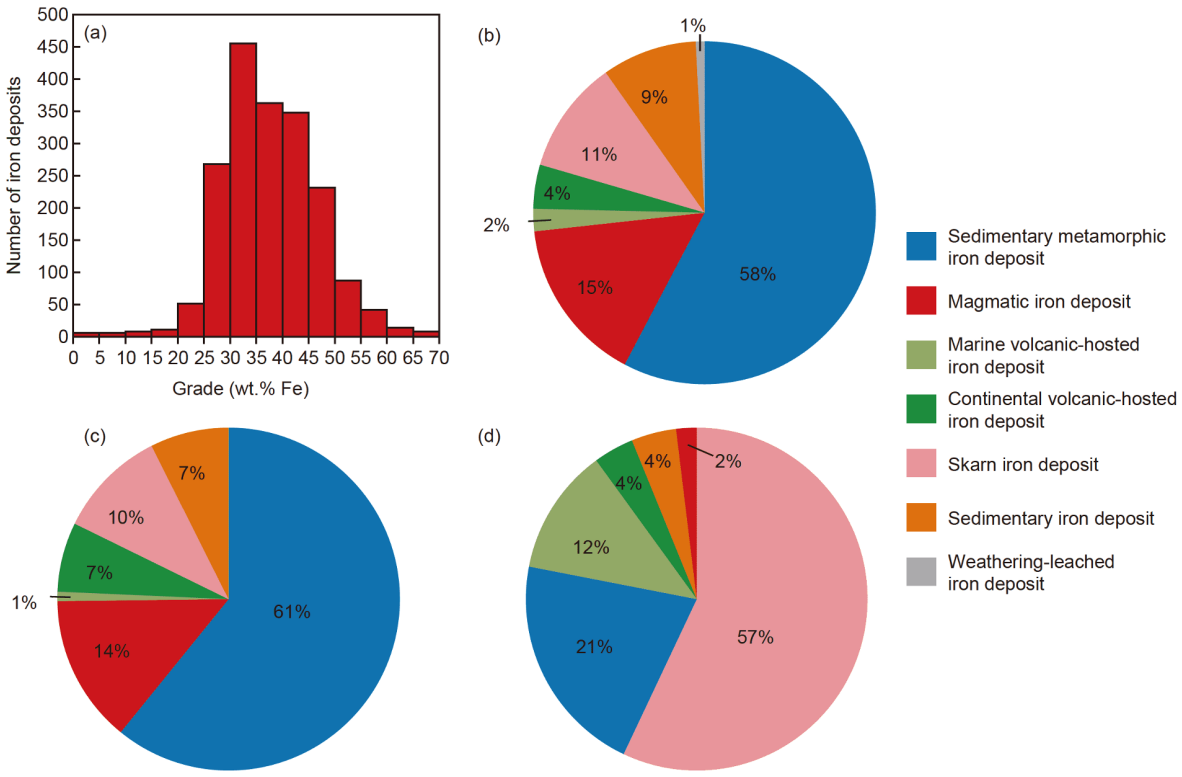

Figure 1 Statistics of iron ore resources in China. (a) Histogram of Fe grades of iron deposits in China; (b) total iron ore resources of different types of iron deposits in China; (c) statistics of large iron deposits in China (>100 Mt of ores); (d) high-grade iron resources (≥50 wt.% Fe) of different types of iron deposits in China (modified after Zhang et al. (2014a)). Note: Sedimentary metamorphic iron deposit refers to the special BIF-type iron deposits in China.

oxides. With subsequent metamorphism and deformation, these BIFs could be transformed into sedimentary metamorphic iron deposits. Based on their ages, Chinese BIF-related iron deposits can be divided into two groups. (1) Neoarchean-Paleoproterozoic. These deposits are mainly distributed in the North China Craton (NCC), where most important sedimentary metamorphic iron deposits clustered. (2) Neoproterozoic. They are relatively rare and mainly found in South China, for example, Yangjiaqiao iron deposit in Xinyu in Jiangxi Province and Shilu iron deposit in Hainan Province (e.g., Xu et al., 2009; Li Z H et al., 2014; Zhang et al., 2018). Due to the length limitation of the paper, here we only focus on the geological settings of the former case.

BIF-related iron deposit in NCC mostly belong to the Algoma-type which had formed during late Neoarchean period (2.55–2.50 Ga). These Algoma-type BIFs are concentrated in the eastern part of NCC including Anshan-Benxi area in Liaoning Province, eastern Hebei Province and Western Shandong Province. Geographically, the locations of these iron deposits formed a large arc-shaped sedimentary metamorphic iron ore metallogenic belt (Zhang et al., 2012a, 2012b). Current research shows that most BIFs were initially precipitated during 3.8–1.8 Ga under an anoxic and iron-rich ocean environment (Bekker et al., 2010; Konhauser et al., 2017). Li Y H et al. (2014) reported positive δ^{56}Fe values for all these BIFs, and in combination with the obvious mass-independent sulfur isotope fractionation, they suggested that these BIF-related iron deposits in NCC formed under relative anoxic submarine circumstances. Their study also indicates that during the early period of the GOE, the sea water had not yet been oxidized, thus formed a redox-stratified ocean with oxidizing superstratum and reducing substratum. Li H M et al. (2014a) thus suggested that the BIF in NCC were formed under shallow marine environment based on case studies on Gongchangling iron deposit in Liaoning Province and Wuyang iron deposits iron deposit in Henan Province. According to the discussions above, we propose that the late Neoarchean BIF-related iron deposits in NCC were formed as follows.

(1) During the Mesoarchean-Neoarchean period, the ancient continental crust was thin, and ocean basins were relatively easy to be generated by extension. Under such environment, relatively Fe-rich mafic-ultramafic primitive magmas erupted onto the sea floor by submarine volcanism. Due to the anoxic atmosphere, the upper part of the ocean was still quite reduced. Sea water circulation triggered by syngenetic fault earthquake pump could leach large volume of Fe from the juvenile oceanic crust as Fe^{2+} due to relative reducing condition (Figure 3a).

(2) During the initial stage of the GOE, up-flow of sea water by circulation will carry large amount of dissolved Fe^{2+} into the redox interface. Consequently, Fe^{2+} will be effi-

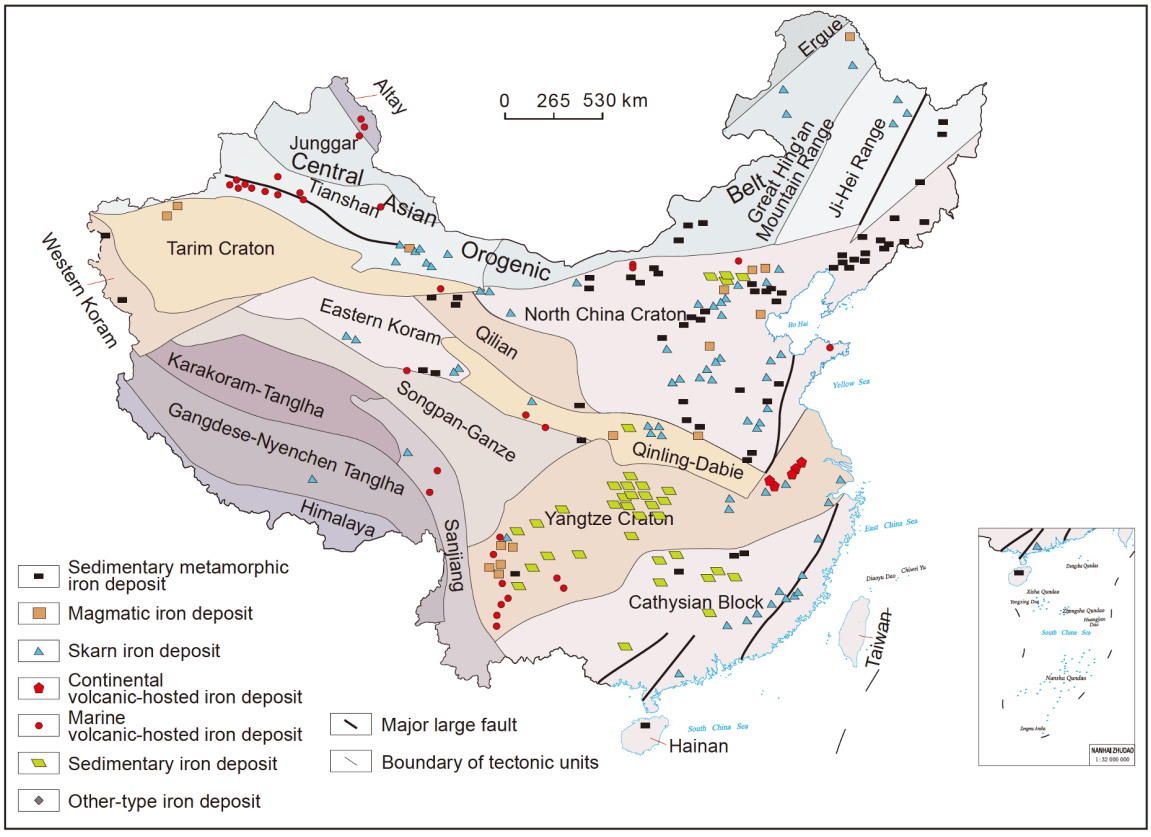

Figure 2 Distribution of the iron deposits in China (modified after Zhang et al. (2014a)). Note: The weathering-leaching type in Figure 1 is classified into the other types in Figure 2.

ciently oxidized into Fe^{3+}, leading to the formation of BIFs (Figure 3b). This model can plausibly explain the characteristics of the BIF-related iron deposits in NCC, such as precipitation at shallow sea, short duration of iron mineralization, and redox-stratified sea water as revealed by fractionation of Fe and S isotopes, etc.

3.1.2 Geological setting of skarn and continental volcanic-hosted iron deposits

Skarn and continental volcanic-hosted types of iron deposits in China are predominantly distributed in two areas. One is the Middle-Lower Reaches of the Yangtze River Metallogenic Belt and the another one is the East Block of NCC (Figure 2). Accordingly, the skarn-type iron deposits are found to be concentrated in three ore clusters including: (1) the Daye ore cluster in the Middle and Lower Reaches of the Yangtze River Metallogenic Belt, (2) Laiwu, Zibo and Jinan ore clusters in the eastern block of the NCC, and (3) Han-Xing and Linfen ore clusters in the Central Orogenic Belt in NCC. In contrast, the continental volcanic-hosted type iron deposits are mostly restricted in the Ningwu and Luzong volcanic basins in the Middle-Lower Reaches of the Yangtze River Metallogenic Belt. Interestingly, the distribution of these ore clusters shows strong genetic correlation with the regional deep fault system. For example, the Daye, Luzong and Ningwu ore clusters are distributed in western, middle and eastern segments, respectively, of the Middle-Lower Reaches of the Yangtze River Metallogenic Belt, along the same direction with the Yangtze River deep faults (e.g., Zhai et al., 1992; Chang Y F et al., 2019). Besides, Laiwu, Zibo and Jinan ore clusters are uniform with Tanlu NW-trending secondary fault which belong to the R' fault system according to the strike-slip fault system proposed by Wilson et al. (1973). Moreover, the Han-Xing and Linfen ore clusters in the Central Orogenic Belt of the NCC are distributed in association with a series of NW-trending faults, which are called Taihang Mountain piedmont faults. These piedmont faults strike almost parallel to the Central Orogenic Belt in the NCC, which had been believed to be formed by the collision between western and eastern blocks of NCC during the Paleoproterozoic (Zhao et al., 2001).

Numerous high-precision geochronological studies had shown that both skarn and continental volcanic-hosted iron deposits in eastern China were extensively formed at *ca.* 130 Ma (e.g., Deng et al., 2014, 2015, 2017; Li J W et al., 2014; Xie et al., 2015; Zhou et al., 2017). The previous studies had also shown that during 130 Ma, the tectonic regime of eastern China was converted from compression to extension (e.g., Chen B et al., 2008; Sun et al., 2008; Mao et al., 2011; Zhou et al., 2017). In an extension regime, decompression

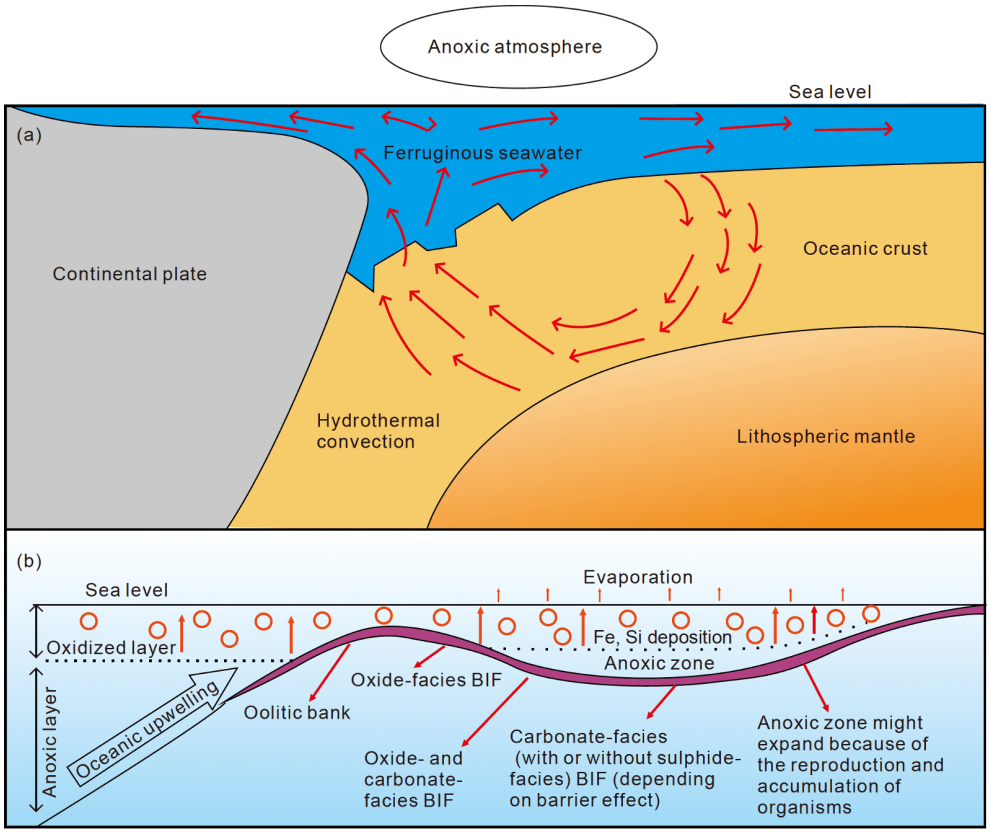

Figure 3 Cartoon model for the formation of BIF-related iron deposits in NCC. (a) Anoxic environment in Mesoarchean-Neoarchean brought huge amount of Fe^{2+} in the sea water; (b) during the early period of GOE, circulation of sea-water carried dissolved Fe^{2+} to the interface of reduction-oxidation leading to the formation of BIFs (modified from Li et al. (2012)).

partial melting of sub-continent lithospheric mantle (SCLM) in both NCC and YC occurred, while the deep faults were also developed, including Yangtze River deep faults, Central Orogenic Belt and Tanlu fault zone, leading to extensive magmatism. The intermediate-acid and intermediate-mafic intrusions were thus formed by magmatic differentiation, e.g., fractional crystallization, magma mixing and crustal contamination from primitive magmas (Chen et al., 2007; Chen B et al., 2008; Li et al., 2009; Xie et al., 2015). Furthermore, the extension would also cause rapid decompression of the ore-forming magmas, thus strongly decreased the solubility of volatiles in the melts, which is a favourable condition to release iron-rich mineralizing fluids by exsolution. Besides, the host rocks of these skarn and continental volcanic-hosted iron deposits are commonly associated with big plutonic complex, and their formation involves multiple pulses of emplacement of magmas from depth (e.g., Zhai et al., 1992; Chen B et al., 2008; Li J W et al., 2014). Multi-stage emplacement of magmas could maintain a prolonged molten state of the magma chamber and provide abundant fluids by exsolution, which is the key factor for the formation of the large-scale skarn-type high-grade iron deposits (Li W et al., 2019).

3.1.3 Geological setting of submarine volcanic-hosted iron deposits

Submarine volcanic-hosted iron deposits have been recognized to be distributed in Western China (Figure 2), including Awulale in Western Tianshan, Eastern Tianshan, Northern margin of Eastern Junggar, southern margin of Altay, Kaladawan area at eastern part of the Altyn Tagh Mountain and southwestern margin of Yangtze Block (Dahongshan and Etouchang). During the past decades, several large-scale submarine volcanic-hosted iron deposits (e.g., Beizhan, Chagangnuoer, Zhibo and Dunde) and a series of medium- and small-scale iron deposits have been discovered in Awulale, western Tianshan where high-grade iron ores dominate in these deposits. Recent geochronological studies indicate the ore-bearing volcanic rocks and iron ores formed during 330–310 Ma. The geochemical characteristics of volcanic rocks suggest a continental arc margin setting for this type of iron deposits (e.g., Duan et al., 2014; Yang et al., 2013; Wang X S et al., 2018). However, why do most of the continental arc margins lack the endowment of submarine volcanic-hosted iron deposits?

Zhang et al. (2016) proposed the positive $\varepsilon_{Nd}(t)$ values of the volcanic rocks associated with the iron deposits are related to the fractional crystallization of the magmas derived

from depleted asthenospheric mantle rather than partial melting of oceanic crust or continental crust directly. Particularly, the partial melting of asthenospheric mantle, not oceanic crust or continental crust could be related to the "hot mantle-cold crust" thermal structure, i.e., high-density oceanic crust subducted in high angle in the subduction zone (Figure 4). Hence, the dehydration of the oceanic crust contributes to the partial melting of asthenospheric mantle that induces iron-rich mafic primitive magma, making it potential for the enrichment of iron during the later stage. Furthermore, the high-angle subduction model in the "hot mantle-cold crust" subduction zone could also readily explain the geological characteristics of the submarine volcanic-hosted iron deposits. For example, the high-salinity magmatic hydrothermal fluids are related to the fractional crystallization in the magma chamber during subduction, whereas the mixing of magmatic hydrothermal fluids and seawater during mineralization is related to the infiltrated seawater under the extensional setting. This specific tectonic setting could account for the rare occurrence of submarine volcanic-hosted iron deposits in the world as well.

3.1.4 Geological setting of magmatic iron deposits

Distinctive from other types of iron deposits, magmatic iron deposits are also the main sources for Ti and V. According to the host rock association, they can be subdivided into two categories. One is related to Proterozoic anorthosite massif that has only been recognized at Damiao-Heishan in Chengde, NCC during *ca.* 1.8–1.7 Ga, and thus also known as Damiao-type iron deposits. The other one type is Fe-Ti-V oxides deposits associated with layered mafic intrusions which are widely distributed in China. However, the most economically valuable Fe-Ti-V oxide deposits are clustered in the Panxi region, making this region the world's largest Fe-Ti-V oxides ore cluster. It is broadly accepted that the Damiao-type iron deposits were formed in a post-collisional extension environment (e.g., Duchesne et al., 1999; Zhang et al., 2007; Vander Auwera et al., 2011).

Panxi region lies in the inner zone of the Emeishan large igneous province (ELIP). The distribution of the Fe-Ti-V oxide deposits in this region is controlled by major N-S trending faults and is closely related to the activities of the Permian (~260 Ma) Emeishan mantle plume. It has been revealed that the composition of the parental magma of the representative Panzhihua ore-bearing layered intrusion is ferrobasaltic (e.g., Zhou et al., 2005; Zhang et al., 2009; Hou et al., 2011; Bai et al., 2013; Song et al., 2013). Based on study on the picritic dikes in the Panzhihua, Hou et al. (2013) proposed that the primary magma was ferropicrite. Although ferropicritic melt can be formed by partial melting of the

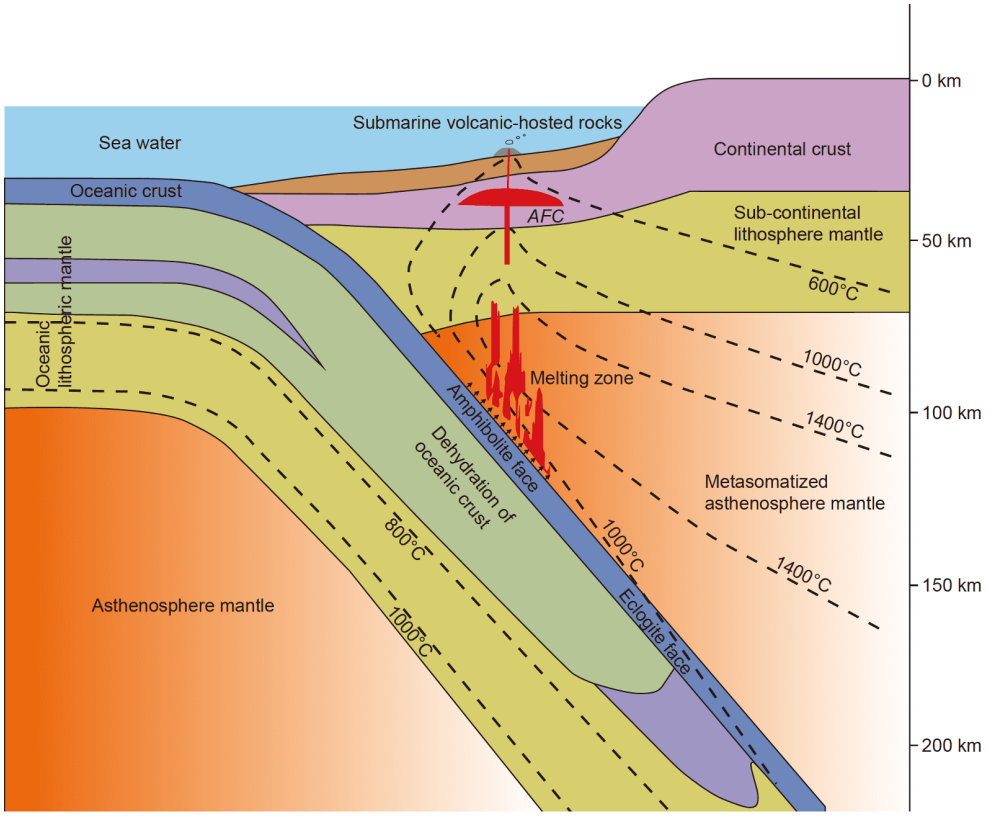

Figure 4 The cartoon image for the tectonic setting of the submarine volcanic-hosted iron deposits (modified from Zhang et al. (2016)). High-angle subduction of oceanic crust lead to the partial melting of asthenospheric mantle in the "hot mantle-cold crust" subduction zone. The fractional crystallization of the ascending mafic magma in the magma chamber could form iron-rich magmatic fluids, which promote the iron mineralization in the later stage. AFC refers to assimilation and fractional crystallization.

mantle under high pressures (e.g., Xu et al., 2001), it should be noted that such melts ought to be also enriched in alkalis (Zhang et al., 2006) due to small degree of partial melting. However, obviously this is not the case for the ore-forming parental magma in the Panxi region (Zhang et al., 2009). On the other hand, experimental study (e.g., Tuff et al., 2005) also had shown that the production of ferropicritic melt requires not only peridotite but also Fe-rich components such as eclogite or pyroxenite in the mantle source. Accordingly, Hou et al. (2011, 2013) advocated that the mantle source beneath the Panxi region contains subduction-related components based on the olivine and clinopyroxene noble gas isotopes in the four typical ore-bearing intrusions including Hongge, Panzhihua, Taihe and Baima and the Re-Os isotopes of picritic dikes in Panzhihua. These conclusions are in agreement with the low clinopyroxene ^{18}O isotopes (<5.5‰) of the Panzhihua layered intrusion (Zhang et al., 2009). Therefore, the enrichment of iron in the primary ferropicritic magma is more likely to be derived by the involvement of subduction-related eclogite or pyroxenite in the mantle source (e.g., Hou et al., 2011, 2013; Bai et al., 2014). Combined with the regional geology, we suggest that oceanic lithosphere subducted eastward beneath the Yangtze block in Neoproterozoic (Zhou et al., 2006), and after reaching Panxi area the subduction slab underwent eclogite facies metamorphism. Subsequently the interaction between the subduction-modified lithosphere and the Permian Emeishan plume led them to be partially melted together that generated ferropicritic primary melts, which played an important role in the formation of giant Fe-Ti-V oxides deposits in Panxi region (Figure 5).

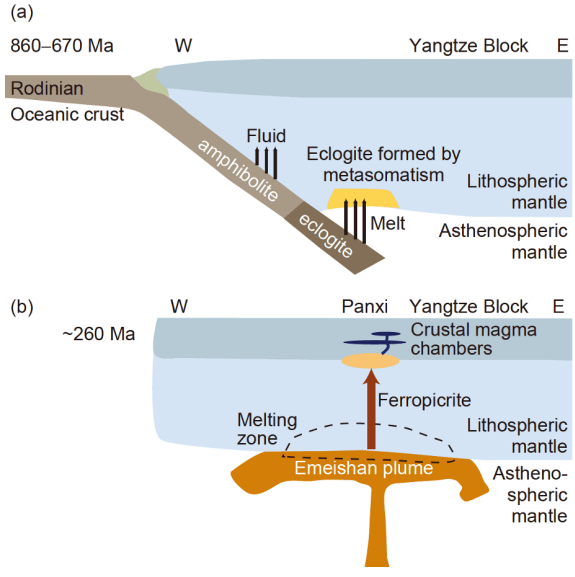

Figure 5 Cartoon image showing the background of the formation of Panxi Fe-Ti-V oxides deposits. (a) Oceanic lithosphere subducted eastward beneath the Panxi area underwent eclogite facies metamorphism; (b) the ascending of Permian Emeishan mantle plume led to the partial melting of eclogite with plume to produce ferropicrite.

3.2 Spatio-temporal evolution of iron deposits in China

The main types of high-grade iron deposits in China are related to the tectonic evolution during different geological periods. BIFs were formed in NCC during the early stage of the GOE during late Archean to early Paleoproterozoic (2.6–2.5 Ga). The Damiao-type magmatic Fe-Ti-V oxide deposit in Chengde area associated with anorthosite massif were formed under the extension in NCC during Mesoproterozoic (~1.7 Ga). Submarine volcanic-hosted iron deposits in western China were formed by the subduction of the oceanic slab during Paleozoic, i.e., the formation of Central Asian Orogenic. The Emeishan mantle plume event formed the world's largest Panzhihua-type magmatic Fe-Ti-V oxide deposit in the Panxi region during Permian. A large number of skarn-type iron deposits and continental volcanic-type iron deposits were formed within a tectonic regime of large-scale lithospheric thinning in eastern China during Mesozoic (~130 Ma; Figure 2).

4. Geological characteristics of high-grade iron deposits in China

4.1 Sedimentary metamorphic high-grade iron deposits

4.1.1 Sedimentary metamorphic high-grade iron deposits related to Neoarchean-Paleoproterozoic BIFs

One notable fact is that the BIF-related iron deposits in China are mainly composed of high-grade magnetite ores (Fe>50 wt.%). Most of these iron deposits are distributed in the Anshan-Benxi area, Liaoning Province (e.g., Li H M et al., 2014a, 2015a; Zhang et al., 2014a, 2015). These high-grade magnetite ore deposits can be classified into two groups with different scales and alteration types. The first group is Gongchangling-type iron deposit, which has 164 Mt high-grade iron ores, mainly reserved in the mining area II of the Gongchangling deposit. High-grade Fe orebodies are mainly hosted in the bedding faults in the BIF, displaying as veins and dikes cutting across the BIF layers. Wallrocks of high-grade orebodies are "altered rocks" containing garnet (e.g., Li H M et al., 2015a; Wang et al., 2012). The contact between the altered rocks and high-grade Fe orebodies is sharp (Figure 6a). There are metasomatic residues of magnetite quartzite in high-grade iron ores (Figure 6b). High-grade massive ores consist of coarse-grained magnetite, minor quartz and chlorite. The second group is medium-small scale Qidashan-type iron deposits, with 11.45 Mt high-grade iron ores, which are mainly distributed in Qidashan, Nanfen, Waitoushan and Donganshan iron deposits. High-grade Fe orebodies are mainly hosted in the bedding faults or collapsed place of folds of the BIF layers, locally in veins/dikes cutting across the BIF layers. Altered rocks in the contact

zone are characterized by presence of chlorite (e.g., Yang et al., 2014; Li H M et al., 2015a), and have a sharp contact with the ore bodies (Figure 6c). Alongside the high-grade ore veins, BIFs disappeared, and changed to quartzite (Figure 6d). High-grade compact massive magnetite ores consist mainly of coarse-grained magnetite with minor martite, quartz, chlorite and tremolite. In recent years, high-grade magnetite ores are also found in some drilling core of deep mineral exploration in the Xingshan iron deposit, Eastern Area of Hebei. The thickness of the iron orebodies in a one bolehole is >100 m (Chen et al., 2010).

Economically important hematite-dominated high-grade iron deposit is rare in NCC and only the Yuanjiacun iron deposit in the Lüliang area in Shanxi Province has been reported. In Yuanjiacun deposit, various scale high-grade hematite orebodies are hosted in the faults in Proterozoic BIFs, with only 4.24 Mt high-grade iron ores (average 53.4 wt.% for Fe). The contact between the hematite orebodies and wallrocks is always sharp. High-grade hematite ores are characterized by banded or massive structure, with slightly banded ores transformed into massive ores locally. In addition, banded ores show obvious porous/vesicular structure, mainly consisting of martite, banded hematite with minor quartz.

4.1.2 Sedimentary metamorphic high-grade iron deposits related to Neoproterozoic BIF—Taking the Shilu iron deposit as an example

Minor Neoproterozoic BIF-type iron deposits are mainly distributed in South China, such as the Xinyu iron deposit in Jiangxi province and the Shilu iron deposit in Hainan Province (e.g., Xu et al., 2009; Li Z H et al., 2014; Zhang et al., 2018). The Shilu iron deposit is taken as an example to illustrate geological characteristics of this kind of iron deposit in China.

The Shilu iron deposit contains proven Fe-ore reserves of more than 500 Mt (average 51 wt.% for Fe), which is the largest high-grade iron deposit in Asia (Xu et al., 2013, 2014). The ore minerals are dominated by hematite with subordinate Co, Cu bearing minerals as by-product. Stratiform or stratiform-like Fe- and Co-Cu orebodies are located at the trough and along the transitional section from limbs to troughs of the NW-trending synclinorium. The iron orebodies are mainly hosted in the Meso- to Neoproterozoic Shilu Group, a suite of nertic or neritic-lagoonal clastic-carbonate succession which has been metamorphosed to greenschist facies (locally up to amphibolite facies). The Shilu Group can be further divided into seven lithostratigraphic sequences from bottom to top. Fe- and Co-Cu ores are mainly hosted by the sixth sequence. In addition to ore-forming minerals, this sequence also comprises banded diopside-tremolite assemblage, banded or ocellar garnet-bearing diopside-tremolite assemblage, banded dolostones, ferruginous phyllites or sandstones (Figure 7a), and locally intercalated with barite, gypsum and jasperite. Intrusive rocks are also abundant in the Shilu ore district, dominated by Indosinian-Yanshanian granites. Late Yanshanian dikes, including granitic porphyries, lamprophyres and diabases, are emplaced mainly along faults or lithological contacts.

The Shilu iron deposit comprises 38 Fe orebodies, 17 Co and 41 Cu orebodies. Vertically, the Fe orebodies are generally located about 30–60 m above the Co-Cu orebodies. The Fe orebodies are generally layered and show lentiform S- or reversed-S-type shapes, which is closely related to tectonic foliations and conjugate shear joints. The deposit is 3525 m along the strike, 463 m in width with a maximum thickness of 430 m. The contact between Fe-ores and their host rocks is generally sharp (Figure 7b). Whereas alongside the brittle-ductile shear faults, strong shearing has smeared the original sharp contact to a more transitional zone from strongly silicified host rocks, via Fe-poor layers to Fe-rich layers (Figure 7c). Based on the content of hematite, the Fe-ores can be divided into Fe-rich ores (Figure 7d) and Fe-poor ores. Ore minerals in the former are dominated by hematite (~85 vol.%), locally with minor magnetite and specular hematite. Gangue minerals include quartz and minor sericite. Fe-rich ores are characterized by lepidoblastic and massive texture. Mineralogy of Fe-poor ores comprise hematite (20–40 vol.%), magnetite (20–45 vol.%), quartz, feldspar, grossular-almandine, diopside, actinolite, epidote, sericite, calcite, dolomite and minor barite. Fe-poor ores generally exhibit massive, banded and ocellar structures with lepidoblastic, blastopsammitic and porphyroblastic textures.

4.2 Skarn-type high-grade iron deposits

The skarn-type high-grade iron deposits mainly occur at the contact zone between the intermediate basic to intermediate acid intrusion and the gypsum-bearing carbonate wall rocks. In addition, some orebodies occur within intrusion as xenoliths, or in the surrounding carbonate but could be hundreds of meters away from the intrusion. The occurrence of the ore bodies shows various shapes, e.g., irregular, tabular, stratified, veined, lensed and sack-like. This scenario reflects that they are mainly controlled by the structure of the intrusive contact zone, brittle fracture, interlayer fracture zone in carbonatic wall rocks and surrounding rock xenoliths (e.g., Zhao et al., 1990; Zhai et al., 1992). Surprisingly, weak wall-rock alteration is observed in the high-grade iron deposits compared with those of low-grade ones. In most cases, at sharp contact with wall rocks (Figure 8a), the thickness of the alteration zone is only several to tens of centimeters. Almost no altered aureole has been observed in some cases, with only spotted phlogopite, epidote, calcite present inside the high-grade ore bodies. Typical examples include: Guangshan, Xiaobaoshan and Naojiao iron deposits in Lingxiang

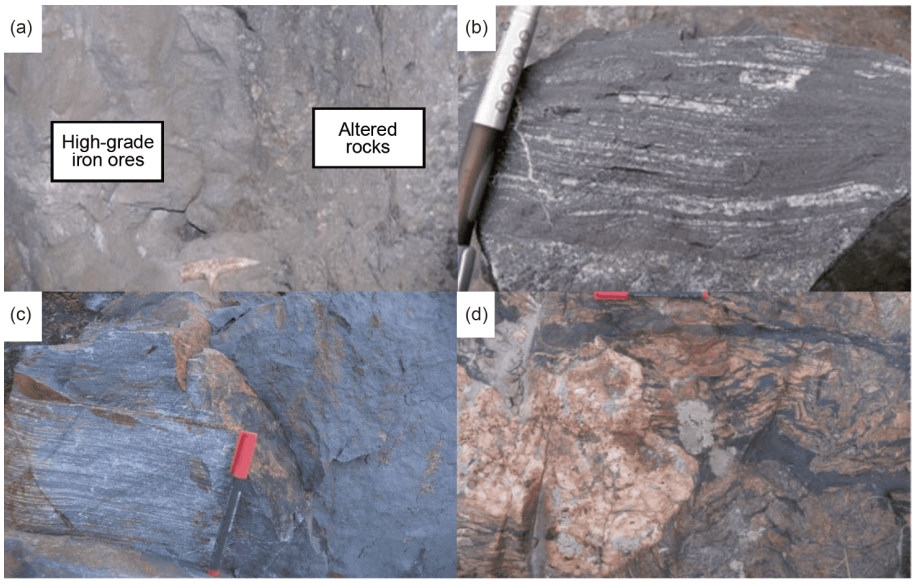

Figure 6 Geological characteristics of high-grade iron deposits in Anshan-Benxi area. (a) Sharp contact between massive high-grade magnetite ores and altered rocks, Gongchangling; (b) metasomatic residues of chert bands of BIF in high-grade iron ores, Gongchangling; (c) sharp contact between massive high-grade magnetite ores and altered rocks, Qidashan; (d) BIFs are replaced by magnetite-lost quartzite and crosscutting high-grade ore veins, Qidashan.

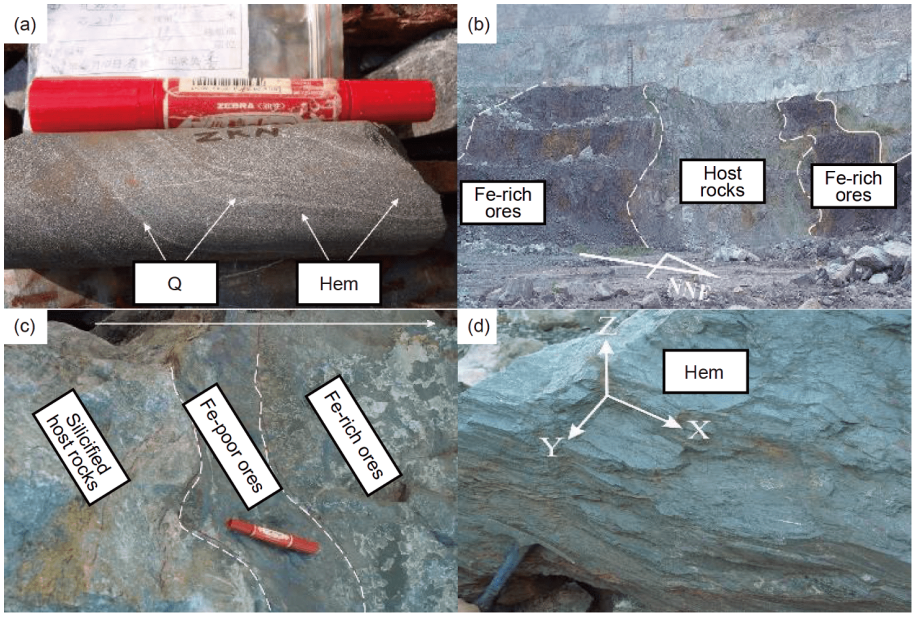

Figure 7 Geological characteristics of the Shilu iron deposit. (a) Fe-poor ores consist of alternating quartzite and hematite quartzite bands; (b) sharp contact between high-grade iron ores and wallrocks; (c) transitional zone from strongly silicified host rocks, via Fe-poor ores to Fe-rich ores; (d) massive Fe-rich ores. Hem-hematite; Q-quartz.

ore field in Daye ore cluster, orebody III of the Chengchao iron deposit, Xiangbishan, Jianshan and Tiemenkan orebody of the Tieshan iron deposit, #1 ore section of the Zhangjiawa iron deposit in Laiwu, #1 and #2 orebodies of the Xishimen iron deposit in Han-Xing region, etc. The high-grade iron ore in these ore bodies usually display massive, veined, powdery (Figure 8b), porous, and brecciated structures, which are significantly different from the disseminated and taxitic structures of the low-grade iron ore bodies. Magnetite (up to >90 vol.%) is the predominant mineral in all high-grade iron ores, with minor hematite. Minor gangue minerals are diopside, sodium feldspar, scapolite, epidote, pyrite, quartz and calcite (e.g., Shu et al., 1992; Zhai et al., 1992).

In Chengchao and Zhangjiawa iron deposits (e.g., Zhao et al., 1990; Chang Z S et al., 2019), the amount of high-grade iron ore is relatively small. It is worth noting that these high-grade ores are characterized by development of magnesian or

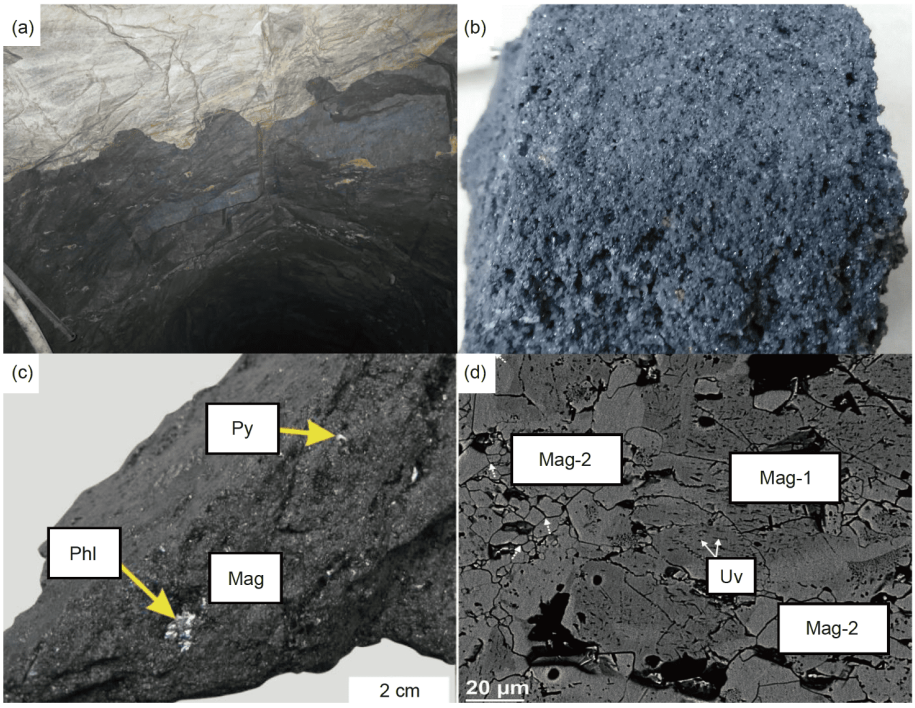

Figure 8 (a) Skarn-type high-grade iron ore in sharp contact with surrounding rocks, Daye Iron Mine, Hubei; (b) vesicular ore, Xishimen Iron Mine, Handan, Hebei; (c) phlogopite in high-grade iron ore, Zhangjiawa Iron Mine, Laiwu, Shandong; (d) backscattering image of magnetite re-equilibration texture, Daye, Hubei (Hu et al., 2015). Mag-magnetite (numbers in the figure represent stages of magnetite); Phl-phlogopite; Py-pyrite; Uv-ulvöspinel.

Mg-rich Ca-Mg skarn, in which magnesian spinel, forsterite, diopside, humite, phlogopite and serpentine are common (Figure 8c). Besides, the presence of magnesian skarn is consistent with the Mg-rich sedimentary wall rocks, i.e., dolomitic limestone. Moreover, since the magnesian skarn minerals are almost iron free, thus the dissolved iron in hydrothermal fluids will be precipitated during the retrograde of the skarn, which is a favourable condition for the formation of high-grade iron ores. These magnetites are usually chemically homogenous without any zonation, and characterized by enrichment in Mg. In contrast, those magnetites associated with calcic skarn-type high-grade iron deposits are chemically zoned and enriched in Si, Al and Ca, etc., instead. (e.g., Hu et al., 2014a, 2014b, 2015, 2017, 2020; Yang et al., 2017; Liu et al., 2019). Besides, magnetite in magnesian skarn commonly co-exists with geikielite, ilmenite, manganilmenite, corundum, rutile and other oxides, and exsolution of fine-grained magnesian spinel can be observed in these magnesian skarn-type high-grade iron ores. Magnetite in skarn-type high-grade iron ores often display various texture including re-equilibration (Figure 8d), vesicular, spongy and irregular island textures. These textures have reflected that the magnetite had been multiply metasomatized by late-stage hydrothermal fluids, in which the concentration of iron had been gradually enriched by leaching (Hu et al., 2014b). Low-grade skarn-type iron deposits, e.g., Wangbaoshan in Daye ore cluster, lack such texture in its magnetite (Hu et al., 2020).

4.3 Volcanic-hosted high-grade iron deposits

4.3.1 Continental volcanic-hosted high-grade iron deposits

Generally, continental volcanic-hosted high-grade iron deposits are both temporally and spatially related to the coeval (sub-)volcanic rocks. According to the occurrence and nature of the wall rocks, these iron deposits could be classified into two types.

(1) The first type occurred in subvolcanic rocks and volcanic rocks, e.g., Meishan, Niushoushan, Washan, Dadongshan and Taocun in Ningwu basin and Nihe and Luohe in Luzong basin. The orebodies mainly show lense, bell and vein-shaped, which are mainly controlled by the structure at contact zone, particularly the fractures and collapse due to condensation. Hence, the main orebodies could occur in the dioritic porphyry and also in the volcanic wall rocks (pyroxene andesite for instance). Massive ores are composed of near pure magnetite (Research Group of Ningwu, 1978) with minor apatite, diopside, actinolite, etc. The high-grade ores are characterized by the mineral assemblage of magnetite-apatite-diopside (actinolite), which is consistent with typical IOA (iron oxide-apatite) deposits worldwide. Predominant alteration minerals consist of diopside, garnet, marialite and chlorite (Chang et al., 1991; Fan et al., 2010), and formed unique "gypsum-pyroxene" and "gypsum-garnet" assemblage (Huang and Yin, 1989) in Meishan, Luohe and Nihe iron deposits.

Another type usually occurred at the contact zone between subvolcanic intrusions and pre-volcanic rock series (wall rocks). Typical deposits include Gushan, Fenghuangshan and Hemushan iron deposits in Ningwu basin. Among these deposits, high-grade iron orebodies are exclusively found at the contact zone between dioritic porphyry and Triassic Huangmaqing Formation (sand shale, siltstone and shale) and Qinglong Group (limestone). The dome structure, brachy-anticline fold, axial rift, and cracks and unconformity in sedimentary rocks control the shape of high-grade iron ore bodies including lense, stratiform-like, bell-like, dendritic and vein-shaped. Highest grade iron ores are massive martite ores (Research Group of Ningwu, 1978) and lower grade ores contain minor apatite and diopside. Those ore bodies associated with limestone contain phlogopite, belonging to typical IOA deposits. Wall rock alteration is characterized by hornfels formed by contact metamorphism, e.g., Gushan iron deposit, which has less superimposition alteration but extensive kaolinization, siliconization and carbonatization are observed (Hou et al., 2009). The wall-rock alteration features of other typical deposits are almost identical with those of continental volcanic-hosted iron deposits.

The magnetite in the two types is characterized by low Ti, with TiO_2 content <1 wt.% in most cases.

4.3.2 Submarine volcanic-hosted high-grade iron deposits

Submarine volcanic-hosted iron deposits are quite unique as some of them develop typical skarn mineral assemblage, even in absence of intrusion in adjacent to the ore bodies and skarn, e.g., Yamansu iron deposit in eastern Tianshan. As featured by its name, the iron ores are commonly hosted by submarine volcanic rocks or in the contact zone between skarns and submarine volcanic rocks. Volcanic rocks consist of lava, pyroclastic and subvolcanic rocks, and most of which are intermediate in composition. High-grade ore bodies hosted in volcanic rocks (i.e., no skarn) generally occur as stratiform, stratiform-like and vein-shaped without development of any obvious alteration and are in sharp contact with wall rocks (e.g., Zhibo and Chagangnuoer iron deposit in western Tianshan, Shaquanzi iron deposit in eastern Tianshan and Abagong iron deposit in Altay (Figure 9a). In contrast, the high-grade iron orebodies hosted by skarn generally occur in lenticular and vein shapes, which are consistent with the occurrence of wall rocks. These high-grade iron ores gradually change into low-grade iron orebodies and skarn and volcanic wall rocks in sequence (Figure 9b), i.e., display gradual contact with wall rocks (Figure 9c). Mineralogically, high-grade iron ores are dominated by magnetite with 45–68 wt.% total Fe, and minor quartz, apatite, calcite, pyrite, K-feldspar, albite, diopside, epidote and garnet, etc. These ores commonly occur as massive and brecciated structure (Zhibo, Chagangnuo'er, Yamansu and Abagong iron deposits; Figure 9d), and flow and vesicular structure (Zhibo, Chagangnuo'er and Abagong iron deposits; Figure 9e). The structures are obviously different from low-grade iron ores characterized by banded, disseminated and brecciated structure (Figure 9h, 9i). Dendritic (Figure 9g) and tabular (Figure 9f) magnetite crystals are commonly present in high-grade iron ores. Diopside are extensively altered in K-feldspar (Figure 9j). Volcanic rocks are commonly replaced (metasomatized) by magnetite or show dissolution-reprecipitation characteristics (Figure 9l) during late stage.

Magnetite from high-grade ore in submarine volcanic-hosted iron deposits is euhedral to subhedral, and characterized by low concentration in TiO_2 (<0.2 wt.%), i.e., obviously lower than that of igneous magnetite (average in 8 wt.%). Experiments show that the concentration of Ti in igneous magnetite is affected by temperature and oxygen fugacity in magma, i.e., higher temperature and lower oxygen fugacity result in crystallization of magnetite with higher Ti content.

In addition, all the skarn which had developed in submarine volcanic-hosted iron deposits are calcic in composition. Nevertheless, the skarn mineral assemblages vary among these iron deposits. Garnet is commonly present in the IX orebody but absent in I orebody in Mengku iron deposit. In Shaquanzi iron deposit in eastern Tianshan, garnet is absent with epidotite, and skarns are commonly developed. Besides, the shape, texture and composition of these garnet show distinct compositionally variation. For instance, early-formed garnet is fine-grained andradite, whereas late-formed garnet is grossularite-andradite with oscillatory chemical zonation or coarse-grained homogeneous grossularite.

4.4 Magmatic high-grade iron deposits

4.4.1 Panzhihua-type high-grade iron deposits

The Fe-Ti-V oxide deposits in the Panxi region, e.g., Panzhihua, Hongge, Baima and Taihe, are distinctive as the major Fe-Ti-V oxide ore layers (the ore bodies) occur in the lower and middle zones of the layered intrusions, instead of occurring in the upper part in most cases worldwide. Moreover, the majority of these Fe-Ti-V oxide deposits are dominated by disseminated ores. Nevertheless, considerable amounts of high-grade of massive Fe-Ti-V oxide ore layers have been recognized in Panzhihua and Hongge deposits.

These massive ore layers in Panzhihua intrusion with thickness of 40–60 m, mainly found in the lower part of the cycles II and V in the Lower Zone. Sharp contact is observed between high-grade orebody and both gabbro and low-grade iron oxide orebodies (Figure 10a). Laterally stable magnetite gabbro layers with thickness of 10–30 cm are commonly intercalated within the massive ores, forming rhythmic layers. Notably, cumulus silicate minerals in these interlayers are preferentially orientated (Figure 10b). High-grade ores

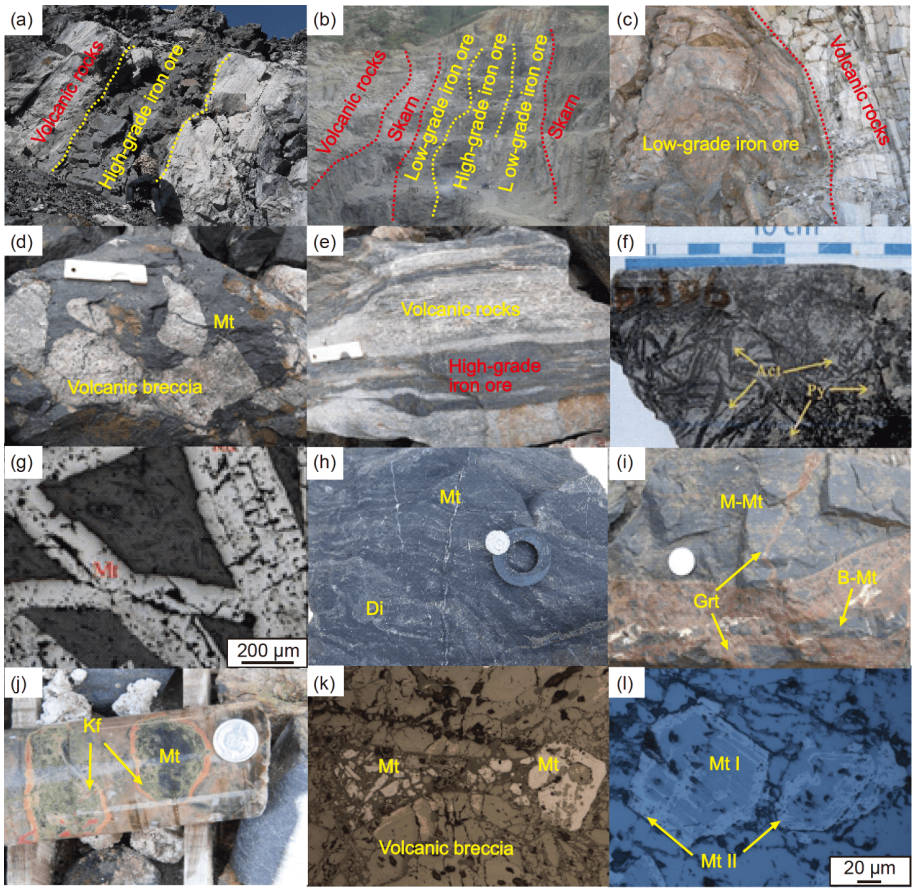

Figure 9 Geological and petrographic characteristics of submarine volcanic-hosted high-grade iron deposits. (a) Volcanic-hosted orebodies occur in stratiform structure, in sharp contact with wall rocks, Jibote iron deposit in Altay. (b) High-grade skarn-hosted iron orebodies are in gradually contact with low-grade orebodies, skarns and volcanic rocks, Mengku iron deposit in Altay. (c) Low-grade skarn-hosted iron orebodies occur in lenticular structure, in sharp contact with wall rocks, Mengku iron deposit in Altay. (d) The volcanic rock breccia is cemented by magnetite, Abagong iron deposit in Altay. (e) Magnetite ores show flow structure. Vein-shape orebodies are in sharp contact with wall rocks, Abagong iron deposit in Altay. (f) Magnetite with tabular texture, Zhibo iron deposit in western Tianshan (Jiang, 2014). (g) Rough surface of the tabular magnetite, Zhibo iron deposit in western Tianshan (reflected-light, Zhang (2013)). (h) Low-grade skarn-hosted orebodies show banded structure, Yamansu iron deposit in eastern Tianshan. (i) Brecciaous ores in low-grade skarn-hosted orebodies and magnetite breccia in garnet skarn, Yamansu iron deposit in eastern Tianshan. (j) Low-grade skarn-hosted iron orebodies show intensively K-feldspar alteration. (k) Volcanic rocks metasomatized by magnetite in low-grade orebodies (reflected-light). (l) BSE images show two-stage formation of magnetite. Abbreviations: Mt-magnetite (I and II represent the early and late stage); Kf-K-feldspar; Di-diopside; Py-pyrite; Act-actinolite; Grt-garnet.

are composed of up to 85 vol.% Fe-Ti oxides, less than 10 vol.% olivine+clinopyroxene and approximately 2–3 vol.% interstitial pyrrhotite and pentlandite. Magnetite occurs as medium-size cumulus crystals or granular crystal aggregate, accounting for 85–90 vol.% of the total Fe-Ti oxides. Besides, ilmenite, accounting for 10–15 vol.% of the total amount of Fe-Ti oxides, usually occurs as euhedral or subhedral and medium- to fine-grain-sized crystals, with extensive exsolution lamella. Cumulus silicate minerals show resorbed texture (Figure 10c) and rimmed by hornblende and olivine. Additionally, exsolution of ilmenite lamella is often observed in cumulus clinopyroxene. Wall rock alteration is generally absent.

4.4.2 Damiao-type high-grade Fe-Ti-P deposits

Damiao-type high-grade Fe-Ti-P deposits refer to the Fe-Ti-P-rich ores occurring as veins and dike swarms in the internal fracture/faults of the Damiao anorthosite in Chengde, Hebei Province (Figure 10d). The Fe-Ti-P-rich vein swarms are clustered in Heishan-Dongdawa sections, including at least 89 orebodies. All of these ores belong to Fe-Ti-P-rich ores and are composed of titanomagnetite, ilmenite and apatite in various proportions (Figure 10e), and basically silicate minerals free.

The high-grade Fe-Ti-P orebodies occur as irregular veins and dikes with variable size in the anorthosite (Figure 10d), with maximal thickness, length and depth of 50, 250 and 200 m, respectively (Sun et al., 2009). The contact between orebody and the surrounding anorthosite is sharp (Chen et al., 2014). Wall-rock alteration is characterized by secondary chlorite on both sides of the orebodies. The width of the alteration aureole is proportional to the scale of orebody, and thus provides an important indicator for prospecting (Zhai, 1965). In terms of mineral content, the upper portion and the

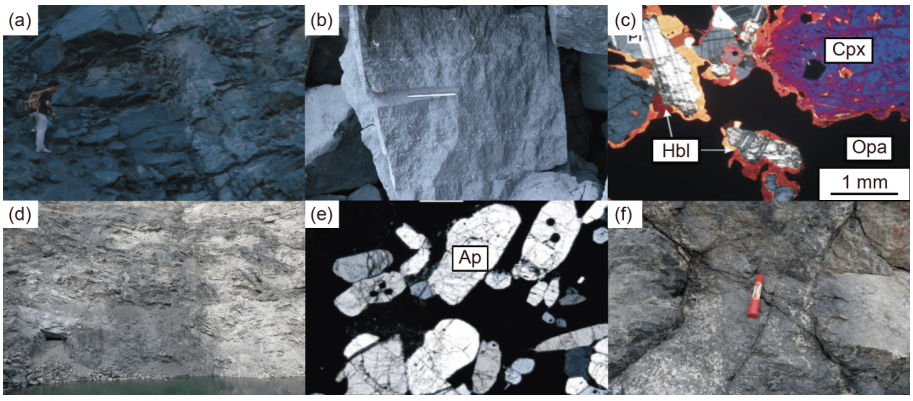

Figure 10 Geological and petrographic characteristics of magmatic high-grade iron deposit. (a) Distinct contact boundary between high-grade iron orebody and gabbro, Panzhihua, Sichuan; (b) high-grade iron ores are intercalated with magnetite gabbro, in which cumulus minerals are preferentially orientated, Panzhihua, Sichuan; (c) the margin of silicate minerals in iron-rich ore is eroded (crossed-polarized light), Panzhihua, Sichuan; (d) the high-grade iron ore veins cut anorthosite, Damiao, Hebei; (e) photomicrographs of the typical iron ore composed of Fe-Ti oxide and apatite (crossed-polarized light), Damiao, Hebei; (f) mineralization zoning of apatite in the rim and iron ore in the core, Damiao, Hebei. Abbreviations: Cpx=clinopyroxene; Hbl=hornblende; Opa=opaque mineral; Ap=apatite.

marginal zone of the orebody is featured by high content of apatite which is up to 70 vol.%, whereas in the middle and lower portion, apatite content is usually minor (<5 vol.%). Notably, the transition in term of apatite content in the ores is not regular, i.e., both gradual and sharp transition could be observed (Figure 10f). Besides, the high-grade Fe-Ti-P ore-veins and Fe-Ti-P-rich silicate dikes are cutting each other, showing a close spatial association. Particularly, at the contact zone between the two types of dikes, gradually transition in crystal mode is observed, as increase in pyroxene and plagioclase plus decrease in Fe-Ti oxide and apatite gradually towards the Fe-Ti-P-rich silicate dikes (Li L X et al., 2010, 2015).

5. Genesis of high-grade iron ores

5.1 Sedimentary metamorphic high-grade iron ores

5.1.1 Sedimentary metamorphic high-grade iron deposits related to Neoarchean-Paleoproterozoic BIFs

For sedimentary metamorphic magnetite-dominated high-grade iron ores, two types are recognized, i.e., Gongchangling and Qidashan types, in Anshan-Benxi region (Liaoning Province). Despite obvious difference in geological characteristics, they still share many similarities as their orebodies are coherently controlled by regional structure and extensive alteration. These features suggest that both types of high-grade iron deposits are product of BIFs (~30 wt.% Fe) altered by fluids (e.g., Zhou, 1994; Zhao, 2013; Li Y H et al., 2014).

Recently, the age of Gongchangling-type iron deposits had been precisely dated at ~1.86 Ga (e.g., Li H M et al., 2014b; Li L X et al., 2019a; Sun et al., 2020). This age is quite close to that of the regional extensive felsic magmatism (~1.85 Ga), indicating the mineralization is genetically associated with extension in the end of Paleoproterozoic, rather than the regional metamorphism and migmatization at 2.50 Ga as previously thought (Li H M et al., 2014b; Li L X et al., 2019a). Notably, the origin of Gongchangling-type is still debated, as two contentious models had been proposed. One is called "desiliconization and iron enrichment", i.e., silica was removed from the BIFs by fluid and leave magnetite undisturbed to form high-grade iron ores. Another is "re-mobilization and re-precipitation of iron" model (i.e., dissolution and migration of iron by hydrothermal fluids and then iron precipitation under favorable conditions), leading to the formation of high-grade iron ores. Currently, the former model is more evidenced in the case of Gongchangling-type: (1) Quartz had been partially replaced by newly-formed magnetite (Figure 6b). (2) garnet occurs adjacent to the high-grade orebodies indicating an alkali-rich environment for alteration (Zhao and Li, 1980). Zhao and Li (1980) experimentally shows reducing fluids with high temperature (500–600°C) and weak alkaline (pH 8–10) could efficiently leach BIFs and dissolve considerable amounts of silica and formed garnet and high-grade magnetite ores. (3) Similar oxygen isotope of magnetite from both high-grade ores and low-grade pristine ores implies that during fluid alteration, iron did not migrate during mineralization (Li H M et al., 2015a). (4) Migration of silica in the fluids will react with Al-rich wallrocks to produce almandite, and with iron-bearing carbonate to produce actinolite and cummingtonite, while the excess silica could be account for the formation of quartz veins and dikes in the deposits. The involving reaction are as follows: SiO_2+aluminum-rich rock→almandite; SiO_2 +iron-bearing carbonate→actinolite+cummingtonite; SiO_2 →quartz vein.

The high-grade magnetite ores of Qidashan-type often occurred at the contact between BIF and granitic migmatite. Hence, most of the researchers believed that the mineralization is genetically related to the ~2.50 Ga tectonic-

magmatic activities (e.g., Zhou, 1994; Yang et al., 2014; Li H M et al., 2015a). Both field and isotopic studies suggest that the mineralization is probably the result of remobilization and re-precipitation of iron, as supported by the following lines: (1) High-grade magnetite orebodies are found as irregular veins cutting across iron-leached BIF, with iron-leached BIF bands developed in the field (Figure 6d); (2) the alteration of wall rocks result in presence of biotite and chlorite, but without garnet, indicating that the alteration process occur under acidic conditions which significantly favor iron migration; (3) the peak value of $\delta^{18}O_{V\text{-}SMOW}$ of quartz in the high-grade magnetite ores is consistent with that in BIF, while the $\delta^{18}O_{V\text{-}SMOW}$ peak value of magnetite in the high-grade magnetite ore is lower than that in BIF, indicating that the iron is re-activated (Yang et al., 2014; Li H M et al., 2015a).

During last century, extensive exploration and genesis research of BIF-type iron deposits were carried out but the results were unsatisfying. Researchers thus attributed this to that NCC did not experience long-term supergene weathering-leaching processes. However, this inference is undermined by the geological characteristics of the Yuanjiacun high-grade hematite deposit. The occurrence of orebody could extend downwards to a depth of 400 m, which is much deeper than that of typical iron deposits with a weathering-leaching genesis (<80 m; Shen and Song, 2015). Fluid inclusions in quartz shows the hematite ore-forming fluids (313–370°C; salinity ~20 wt.% NaCl equiv) derived from depth and migrated upwards along fractures (Li et al., 2020). This indicate the formation of hematite high-grade ores is related to metasomatism, instead of supergene weathering-leaching processes. By comparison, we suggest that, the reason why NCC lack endowment of high-grade hematite ores is probably due to later erosion.

5.1.2 Sedimentary metamorphic high-grade iron deposits related to Neoproterozoic BIF

Compared with typical BIF iron deposits worldwide (e.g., Klein, 2005; Basta et al., 2011), Shilu Fe-Co-Cu ore deposit exhibits complex metallogenic characteristics due to multi-stage structural deformation and related hydrothermal alteration. Therefore, the metal sources, metallogenic epoch, the genetic type of this deposit, especially the enrichment process and mechanism of this high-grade iron deposit, remain controversial. The metallogenic model for the Shilu iron deposit has also been debated, as diverse opinions involving skarn, sedimentary metamorphic (magmatic hydrothermal fluids), sedimentary metamorphic (brine fluids), volcanic-sedimentary metamorphic and hydrothermal IOCG models had been advocated (Xu et al., 2009).

Based on the systematic analysis of the spatial distribution of high-grade iron ore bodies and structural overprinting relationships, Xu et al. (2013) divided the structural deformation and related metamorphism in Shilu mining area into two stages: D1 and D2. The D1 deformation phase is responsible for the formation of the NW-SE trending synclinorium and related ductile shear and high temperature plastic flow; the D2 deformation contains the NE-SW trending shear folds (D2a-b) which superposed on the D1-stage synclinorium, and some large extensional shear detachment fault systems (D2c). The D1 stage involves formation of high-grad iron ore bodies, where iron-polymetallic materials were enriched to the troughs or the transitional section from limbs to troughs of the synclinorium. The D2a-b stage deformation and coeval fluid further redistributed and enriched Fe, Co, Cu and Si at superposed parts of folds. Based on the Sm-Nd isochron ages of 830 and 213 Ma for high-grade iron ores and host rocks, the CHIME-age peaks of 560–440 Ma for monazite and the Ar-Ar plateau age of 132 Ma for actinolite, the structural deformation stages mentioned above can be constrained respectively at 560–450 Ma (D1), 260–210 Ma (D2a-b) and 130–90 Ma (D2c) (e.g., Xu et al., 2009, 2013, 2014, 2015; Wang Z L et al., 2015). Based on the combination of detrital zircon SHRIMP and LA-ICP-MS U-Pb age data and monazite CHIME age data of the host rocks and iron ores, the depositional time-interval of Shilu BIFs and interbedded wall rocks can be constrained at ca. 1075–840 Ma (e.g., Wang Z et al., 2015, Wang Z L et al., 2015; Xu et al., 2015). Therefore, the Shilu iron deposit is the product of a multi-stage evolutionary process, which involves multiple geological processes such as sedimentation, deformation, metamorphism and hydrothermal activity, exhibits typical polygenetic compound deposit characteristics.

Integrated with the geological characteristics and recent geochemical research (e.g., Wang Z et al., 2015; Xu et al., 2015; Yu et al., 2016; Zou et al., 2017), the Shilu iron deposit is considered to be a structurally and hydrothermally re-enriched BIF-type high-grade iron deposit. Xu et al. (2015) proposed a four-stage metallogenic model to account for the genesis of the Shilu deposit: (1) 1075–840 Ma, deposition of interbedded BIFs (Figure 11a); (2) 560–450 Ma, desilicon-ization and iron enrichment of the metal ores caused by the formation of folds, related high-temperature ductile shear and amphibolite-facies metamorphism corresponding to the South China Caledonian orogeny, while magnetite was transferred into hematite (Figure 11b); (3) 260–210 Ma, refinement of the iron deposit through intrusion of granitic magma and structural deformation (Figure 11c); (4) 130–90 Ma, a hydrothermal overprinting mineralization stage (Figure 11d). Among these processes stated above, the second is considered to play the most important role in the formation of high-grade iron orebodies.

5.2 Skarn-type high-grade iron deposits

Based on the temperature estimation of a large amount of

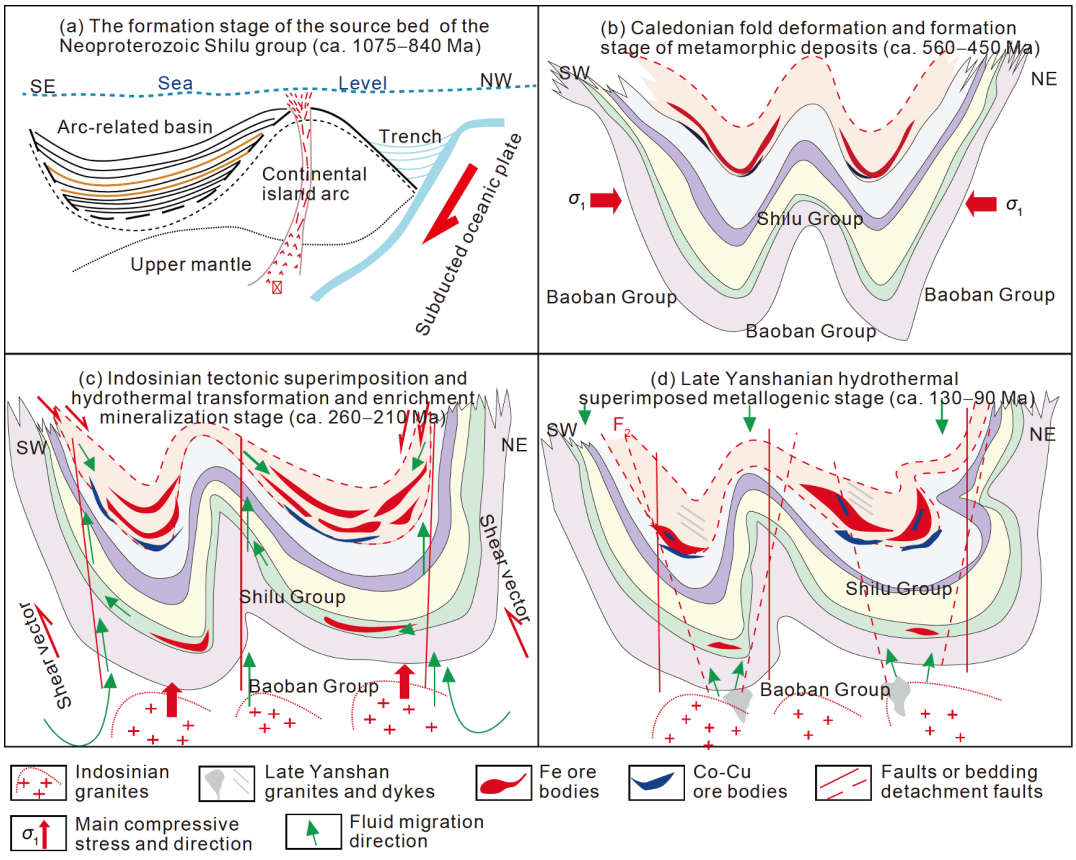

Figure 11 Schematic model illustrating a multi-stage evolution of the Shilu iron deposit (modified after Xu et al. (2015)). The interpretation can be seen in the text.

fluid inclusions in skarn-type high-grade iron deposits, the ore-forming fluids are demonstrated to be high-temperature, high-salinity and Fe-rich magmatic hydrothermal fluids. For example, many fluid inclusions with daughter crystals of hematite, halite, potash, carnallite, anhydrite and some other minerals were found enclosed by early-stage skarn minerals in Chengchao and Tieshan deposits in Daye, indicating that the early-stage ore-forming fluids had high concentrations of both saline and iron (Li W et al., 2019). As reported by Wen et al. (2017), extensive fluid inclusions with pyrrhotite as daughter crystals that are hosted by both the igneous and skarn minerals are developed in the Xishimen iron deposit in Han-Xing region. Based on the volume estimation, the iron contents of these fluid inclusion are up to 12 wt.% (Wen et al., 2017). These fluids inclusions yield homogenization temperatures as high as 600–800°C (Zhai et al., 1992; Li W et al., 2019), suggesting that the ore-forming fluids are characterized by high temperature and thus could be directly exsolved from magmas during the process of fractional crystallization as hydrothermal fluids. Detailed mineralogical studies on the high-grade iron deposits, e.g., Chengchao, Xiaobaoshan, Jianshan and Xiangbishan in Daye, and Zhangjiawa in Laiwu, in addition to magnetite, the high-grade iron ores are also composed of minor spotted phlogopite, epidote and secondary carbonate (i.e., calcite, dolomite and siderite). Generally, quartz, diopside, garnet, fushanite and other skarn minerals are absent. The mineralogy of high-grade iron ores implies the ore-forming fluids are poor in both silica and aluminum, thus unfavorable for development of skarn. This inference is further supported by the presence of geikielite, ilmenite, manganilmenite, rutile and oxides (Zhangjiawa in Laiwu). Essentially, such hydrothermal fluid cannot provide sufficient Si and Al to form skarn minerals, with Ca and Mg from the surrounding rocks during contact metasomatism. Without formation of skarn minerals, the iron in the hydrothermal fluids will eventually be precipitated as magnetite, while the dissolution of the carbonate in wall rocks would result in crystallization of hydrothermal carbonate. We suspect the exsolution of abundant hydrothermal fluids poor in Si- and Al and rich in Fe could be generated due to the prolonged magmatic differentiation caused by multiple magma replenishment.

Many fluid inclusion studies revealed that fluid boiling or phase separation played a key role in the formation of skarn-type high-grade iron deposits (e.g., Zhai et al., 1992). Previous studies had shown that the occurrence of the skarn-type high-grade iron deposits in eastern China are mainly controlled by brittle fractures, interlayer fracture zones, unconformity, brecciated intrusion or folds. Besides, the high-grade iron orebodies generally are in sharp contact with

surrounding rocks, without extensive alteration. Hydraulic breccias are always observed in the wall rocks, with breccias cemented by massive magnetite. Moreover, the "escape structure" of massive magnetite can also be observed in the surrounding carbonate strata (e.g., Yao, 1983; Zhai et al., 1992; Hu et al., 2014a, 2014b; Li W et al., 2019). The above characteristics indicate that these high-grade iron orebodies are not formed by contact metasomatism, but through filling and cooling, precipitation of magnetite of the iron-rich magmatic-hydrothermal fluids in the various spaces created by structural activities (e.g., Yao, 1983; Zhai et al., 1992; Li W et al., 2019). Accordingly, when the high-temperature, high-salinity, iron-rich, Si- and Al-poor magmatic-hydrothermal fluids escape into the various spaces, a tremendous amount of magnetite will be precipitated and separated from the fluids immediately, due to the abrupt decreasing solubility of iron caused by decompression. Most of these high-grade ores are featured by vesicular textures and based on their morphology, some of them are spaces left by the dissolution and migration of some soluble minerals such as carbonate, while others are resulted from rapid escape of volatiles from the ore-forming hydrothermal fluids during the boiling processes. Thus, fluid boiling is recognized as an essential mechanism for rapid precipitation and mineralization of high-grade iron deposits. As discussed above, the magmas having genetic link with skarn-type high-grade iron deposits usually intrudes at relatively shallow level. Thus, when the magmatic fluids were exsolved from these shallow magmatic systems and migrate into the outside structural systems, the corresponding temperature gradient are generally large enough to lead to low solubility of iron and rapid precipitation of magnetite to form iron-rich orebodies (e.g., Whitney et al., 1985). However, on the other hand, the rapid cooling process would limit the formation of contact metasomatism and development of skarn (Meinert et al., 2005).

There is a lot of anhydrite, especially some anhydrite veins in the skarn-type iron deposits, which are recognized as the direct evidences of the involvement of gypsolyte during iron mineralization. As demonstrated by a large number of sulfur isotope data in pyrite (Li et al., 2013), the oxidation of ferrous iron in ore-forming fluids by gypsolyte is another important mechanism of skarn-type iron deposit mineralization. SO_4^{2-} in the gypsolyte has strong oxidizability at high temperature (Pokrovski and Dubrovinsky, 2011), which can play a role as an oxidant and rapidly oxidizes Fe^{2+} into Fe^{3+} in the ore-forming fluids, causing rapid precipitation of magnetite (Wen et al., 2017). Recently, scapolite haloid element and boron isotopes analyses also demonstrate that gypsolyte are actually involved into the formation of Jinshandian skarn high-grade iron deposit in Daye area (Zeng et al., 2019). In addition, the orebodies of high-grade iron deposits have a common feature, that is, the abundant sodium alteration generally occurs in the ore-related magmatic rocks (e.g., Zhao et al., 1990; Zhai et al., 1992). This alteration is associated with the involvement of gypsolyte in magmatic hydrothermal system, which can provide a lot of mineralizer, such as Na^+, Cl^-, and plays an important role in the formation of high-grade iron deposits (Li et al., 2013). When Na^+ in the mineralizing fluids is consumed to form albite, Cl^- can combine with Fe to form the mobile complex (Li et al., 2013). The gypsolyte-rich carbonate wallrocks are mainly composed of dolomite and dolomitic limestone, which can produce the predominant magnesium skarn during contact metasomatism. For example, the wallrock of Zhangjiawa iron deposit, Laiwu, is middle Ordovician dolomite or dolomitic limestone, and the skarn is mainly composed of forsterite, diopside, Mg-spinel, humite, phlogopite, serpentine. These minerals do not contain Fe or have very low Fe contents, indicating that contact metasomatism and skarnization did not consume Fe in the ore-forming fluids. This process can favor the further Fe-enrichment in the fluids and finally precipitation of magnetite, which promotes the formation of high-grade iron deposits.

Diverse re-equilibration textures are well developed in magnetite of skarn-type high-grade iron deposits in eastern China (e.g., Hu et al., 2015; Wen et al., 2017; Li W et al., 2019; Zhu et al., 2019). This scenario indicates that the magnetite had experienced late-stage fluid replacement and modification, which played an important role in the formation of high-quality high-grade iron ores. It is mainly manifested in two cases: (1) The widely developed dissolution-reprecipitation, during which the impurity elements in the primary magnetite are leached and the iron contents are further elevated (Hu et al., 2014b, 2015); (2) Gangue minerals in the magnetite ore are extracted and leached away, which lead to the formation of commonly developed powder-like iron ores, such as in Daye iron deposits. In addition, the multiple-stage magmatic hydrothermal activities can also cause new iron mineralization and multi-phases magnetite, resulting in further enrichment of iron (e.g., Li J W et al., 2014; Li W et al., 2019; Zhu et al., 2019).

Based on the discussion above, the skarn-type high-grade iron deposits in eastern China are mainly formed through several important and continuous processes, including exsolution of the high-temperature, high-salinity, iron-rich, Si- and Al-poor magmatic-hydrothermal fluids, sequentially fluid boiling and rapid cooling, filling and mineralization in the open structural spaces, the involvement of gypsolyte into ore-forming fluids, multi-stage fluid metasomatism and superimposition mineralization.

5.3 Volcanic-hosted high-grade iron deposits

5.3.1 Continental volcanic-hosted high-grade iron deposits

Genetic model of continental volcanic-hosted iron deposits

should be considered together with the genesis of IOA deposits worldwide. IOA deposits are characterized by the volcanic-like ore bodies and the massive ores with lava-like texture and structure (e.g., Park, 1961; Henríquez and Martin, 1978; Song et al., 1981; Nyström and Henriquez, 1994; Henríquez and Nyström, 1998; Naslund, 2002), such as dendritic-shaped, rope-shaped, flow structure and orientation of vesicles in the high-grade iron deposits in Gushan, Anhui province (Chang et al., 1991; Zhai et al., 1992). Therefore, some studies suggested a direct injection of iron ore magma metallogenic model, massive iron oxide ores crystallized from oxide melts (Tornos et al., 2016, 2017). However, this model lacks solid experimental evidence, as previous experimental oxide melts are either obtained in simple system experiments (Naslund, 1983; Li et al., 1986; Yuan, 1990; Lester et al., 2013), or immiscible melts obtained in complex systems but with a much higher temperature (1420°C; Philpotts, 1967). Thus, the significance of those experiments remains contentious. Based on experiments performed in geologically relevant conditions, Hou et al. (2018) first obtained immiscible volatile-rich Fe-Ca-P melts that are compositionally identical to typical IOA ores. Moreover, because of the wetting property of the Fe-Ca-P melt, magnetite and/or apatite are preferentially enclosed in the immiscible Fe-Ca-P melt (Figure 12). The composition of the mixture (i.e., Fe-Ca-P melt+magnetite) resembles that of iron ore magma, which can readily explain the formation of the most high-grade iron ores. However, we have to admit that there will be more or less Ca-, P-bearing impurity components in the "iron ore magma" produced by liquid immiscibility, and the magnetite in the immiscibility experiment has relatively high Ti contents. Thus, for the formation of massive high-grade iron ore which is made up of nearly pure iron oxide minerals with low Ti content, late-stage hydrothermal superimposition and reworking is necessarily required. This inference is expected as extensive hydrothermal alteration had been seen in most of the IOA deposits.

There is a general consensus that the fluids that lead to the hydrothermal alteration and the enrichment process of the ore come from the fluid exsolution during the late-stage of magma crystallization (e.g., Hildebrand, 1986; Zhao, 1993; Sillitoe and Burrows, 2002). However, the nature of this hydrothermal fluids was not well constrained. Our recent studies suggested that this kind of fluid inclusions generally contain hematite and sodium chloride crystals, indicating that the hydrothermal fluid is of high-salinity and Fe-rich (with Fe content up to 12 wt.%). This kind of fluid can not only lead to the hydrothermal alteration such as albitization, but also could rework with the primary magnetite, such as dissolution of the primary magnetite (Hu et al., 2015) and removal of other impurity. Therefore, if possible, the amount of iron in the fluids enriched by 4–5 times will be sufficient to facilitate precipitation of magnetite to form high-grade iron ore.

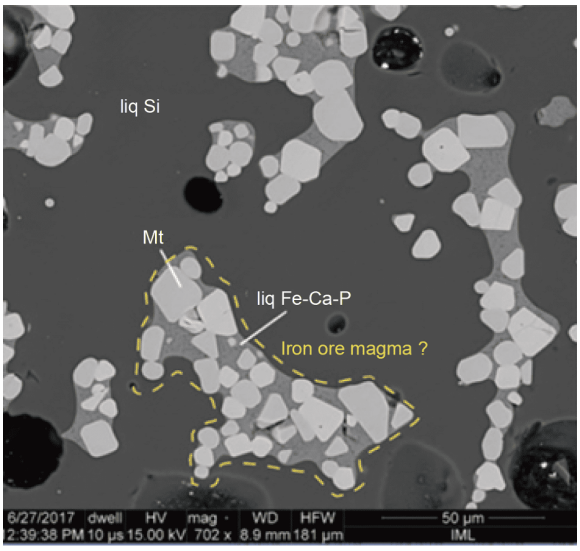

Figure 12 Iron oxide minerals are predominantly enclosed in the Fe-Ca-P melts that are produced by liquid immiscibility; the composition of the mixture is very close to that of high-grade iron ore. Details of the experiments are shown in Hou et al. (2018). Abbreviations: Mt, magnetite; liq Fe-Ca-P, Fe-Ca-P glass; liq Si, Si-rich glass.

In addition, similar to skarn-type iron deposits, the gypsum-bearing carbonate rocks also participated in the mineralization of the continental volcanic-hosted high-grade iron deposits. The main evidences include: (1) The unique "gypsum-pyroxene (gypsum-diopsidite)" assemblage in Luohe, Nihe and Taishan iron deposits is the best evidence for the interaction between dioritic magma and gypsum-bearing carbonate rocks; (2) extensive development of diopside, tremolite, actinolite, albite, marialite, scapolite and K-feldspar indicate that it might be the product of magmatic-hydrothermal alteration of the gypsum bearing carbonate rocks; (3) the $\delta^{34}S$ values for gypsum and sulfide are mostly more than 20‰ and 10‰, respectively, which are much higher than that of the mantle sulfur isotopic range, suggesting that more than 80% of the sulfur in these deposits comes from the gypsum-bearing carbonate (Li et al., 2013); (4) extensive development of sodium alteration is also a common feature of those high-grade iron deposits. The role of gypsolyte had played in the formation high-grade iron ore is similar to that in skarn-type iron deposits.

Conclusively, the continental volcanic-hosted high-grade iron deposits were formed as a result of a combination of multiple segregation of melt with high-temperature, high-salinity and Fe-rich, fluid exsolution and filling and multi-stage superimposition and hydrothermal reworking in the magmatic-hydrothermal system.

5.3.2 Submarine volcanic-hosted high-grade iron deposits

Submarine volcanic-hosted iron deposits have not been reported worldwide, and thus most of the research achieve-

ments were published on Chinese journals (Zhang et al., 2014b). The advocated metallogenic model of these deposits includes volcanic gas-fluid metasomatism-oxide ore melt injection (Lu et al., 1995), magmatic fluid precipitation and metasomatism (Lu et al., 1995; He, 2007), volcanic exhalative sedimentation-hydrothermal reworking volcanic (Chen L C et al., 2008), liquid immiscibility and eruption of oxide ore magma (Zhang and Xie, 2001) and oxide ore melt injection and hydrothermal superimposition (Wang et al., 2006), etc.

Sharp contact between orebodies and wall rocks is quite common in most of these deposits. The iron ores are characterized by explosion brecciated structure, and tabular and dendritic magnetite, which indicate the injection of "pure oxide ore melt or iron-rich fluid" during mineralization (Zhibo, Chagangnuoer, Mengku and Abagong). However, the common development of skarns also indicates the intense alteration which had been caused by hydrothermal fluid metasomatism. This inference is also supported by the low concentration of Ti in magnetite which suggest a hydrothermal in origin. Hence, how high-grade iron orebodies were formed by hydrothermal fluids is still an enigma.

Some volcanic rocks related to these iron deposits are iron-rich. Li N B et al. (2015) reported the ferrobasalts (TFe_2O_3 from 14.55 to 22.68 wt.%) in Chagangnuoer iron deposits in western Tianshan. Li H M et al. (2015b, 2018) discovered iron-rich volcanic breccia and clumps (TFe_2O_3 ~26 wt.%) in Yamansu and Heijianshan iron deposits in eastern Tianshan. Besides, Wang W et al. (2017) found the melts inclusions in the core of the early-stage garnet containing iron-rich melt with magnetite daughter crystals, Jibote iron deposit in Altay. These studies suggest an evolved extremely iron-rich magma which could be formed by differentiation. The enrichment of iron in magma is crucial for the exsolution of iron-rich magmatic fluids during the late stage of solidification. Besides, the coexisting fluid inclusions with melt inclusions contain abundant fluorite, microcrystalline magnetite (Figure 13a) and halite (Figure 13b), indicating a F-rich high-salinity ore-forming fluid. The F-rich high-salinity fluid could leach iron from the iron-rich volcanic rocks, increasing the concentration of iron in the hydrothermal fluid, which had cooled rapidly under large thermal gradient, precipitating magnetite because of the low iron solubility (skarn is absent) or reacted with carbonatite leading to the precipitation of high-grade iron ores (skarns is present).

Magnetite in submarine volcanic-hosted iron deposits show dissolution-reprecipitation characteristics similar to the skarn-type high-grade iron deposits (Figure 9j, 9k). Multiple magnetite and garnet showing various composition have been observed in many submarine volcanic-hosted iron deposits (Jiang et al., 2012; Zhang, 2013). Late-stage magnetite with hydrothermal signature replaced early-stage igneous magnetite by metasomatism (Jiang et al., 2014). Fragment of magnetite ores that are cemented by skarn minerals (Yamansu, Bailingshan, Chagangnuoer and Zhibo iron deposits) has also been observed. The iron-rich ore bodies formed during the late stage suggest the multi-stage of metasomatism and the removal of other element during mineralization. Moreover, multiple pulses of replenishment of primitive magma played an important role in the formation of dissolution-reprecipitation of magnetite in the typical skarn iron deposits as stated above. Accordingly, in this case, we suggest the dissolution-reprecipitation processes for submarine volcanic-hosted iron deposits had also developed which is due to the thermal convection of sea water induced by the active magma chambers.

Zhang et al. (2016) attributed the presence of amphibole and biotite phenocryst in the volcanic rocks to the hydrous nature of the evolved magma. These hydrous magmas could provide sufficient ore-forming fluids to be exsolved, especially under the circumstance that continuous primitive magma replenished into the chamber. Such processes are expected to lead to the dissolution-reprecipitation processes for magnetite, which is crucial for the formation of high-grade magnetite ores.

In summary, for the formation of high-grade iron ore in the submarine volcanic-hosted iron deposits, the following processes are important and necessary: (1) Enrichment of iron in the evolved magma, (2) exsolution of F-rich high-salinity, Fe-rich fluids, (3) continuous supply of such fluids

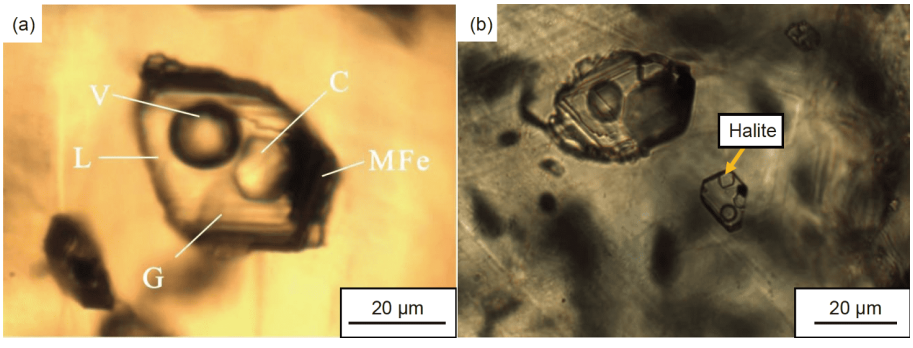

Figure 13 (a) Melt inclusions contain abundant fluorite and microcrystalline magnetite (V-vesicle; G-glass; L-liquid; C-fluorite daughter mineral; MFe-magnetite daughter mineral); (b) halite daughter mineral in fluid inclusion under plane-polarized light in submarine volcanic-hosted iron deposits.

due to primitive magma replenishment in magma chamber, (4) leaching the volcanic rocks by these hydrothermal fluids and formation of Fe-rich ore-forming fluids and (5) metasomatism in low-grade iron ores (removal of the other impurity) to form high-grade iron ores.

5.4 Magmatic high-grade iron deposits

5.4.1 Panzhihua-type high grade iron deposits

This type of iron deposits is generally characterized by dominant low-grade ores, although some of them contain high-grade ores, e.g., the massive orebodies in the Lower Zone of Panzhihua deposit. Currently, the genesis of the high-grade Fe-Ti-V oxide orebodies in the Lower Zone of the Panzhihua layered intrusions remains hotly debated. At least two mechanisms have been mostly invoked to explain the crystallization of the massive Fe-Ti oxide ores. The first one argues for the in-situ crystallization of Fe-Ti oxide from the immiscible oxide liquids that were separated from the Fe-rich magma (e.g., Zhou et al., 2005, 2013a; Liu et al., 2014; Xing and Wang, 2017; Wang K et al., 2018; Cao et al., 2019). In contrast, the second one deciphers the massive orebodies as a result of the gravitational settling of early crystallized Fe-Ti oxide from the Fe-rich silicate magmas (Pang et al., 2008; Zhang et al., 2009). However, both mechanisms are problematic as there is no solid experimental evidence to support the first mechanism whereas the second one cannot readily explain the sharp contact between the massive orebodies and the gabbro. Additionally, Wang M et al. (2017) had identified both Fe- and Si-rich melt inclusions from the apatite and proposed that interstitial liquid immiscibility could occur in crystal mush which was followed by separation of the immiscible conjugates. The Si-rich melts ascended due to their low density, while the magnetite crystallized from the sinking heavier Fe-rich melts. However, this argument still gives no clear explanation for the development of sharp contact between orebodies and wallrocks either.

Petrographic observations suggest that magnetite is the liquidus mineral (Pang et al., 2008) and early-formed cumulus clinopyroxenes generally contain magnetite exsolution lamella, which implies that the parental magma is Fe enriched (Song et al., 2013). This also agrees with the simulated results by MELTs (Song et al., 2013). Besides, the preferential orientation of cumulus minerals in massive ore indicate an origin for flow differentiation (Figure 10b). Therefore, the formation of high-grade orebodies is a result of the accumulation and concentration of early formed Fe-Ti oxide in the flowing magma (Song et al., 2013). In other words, high-grade ore layers were physically segregated from the flowing Fe-rich magma. This has been evidenced by the analogue experiments by Forien et al. (2015). Their experiments revealed that particles (chromite, pyroxene and plagioclase) with various densities can segregate and concentrate in viscous flowing fluids; and the larger difference between the densities leads to the sharper contact between two layers (Figure 14). In the case of Panzhihua deposit, the dominant magnetite is denser than chromite, thus the segregation of massive orebodies and gabbro is more efficient. More importantly, the flow differentiation is also responsible for the various thickness of orebodies in the deposit, e.g., the thick massive orebodies in Zhujiabaobao-Jianshan area are the results of effective segregation and accumulation of the slumped magnetites in the sag of the magma chamber, particularly when the velocity of the magma flow was high.

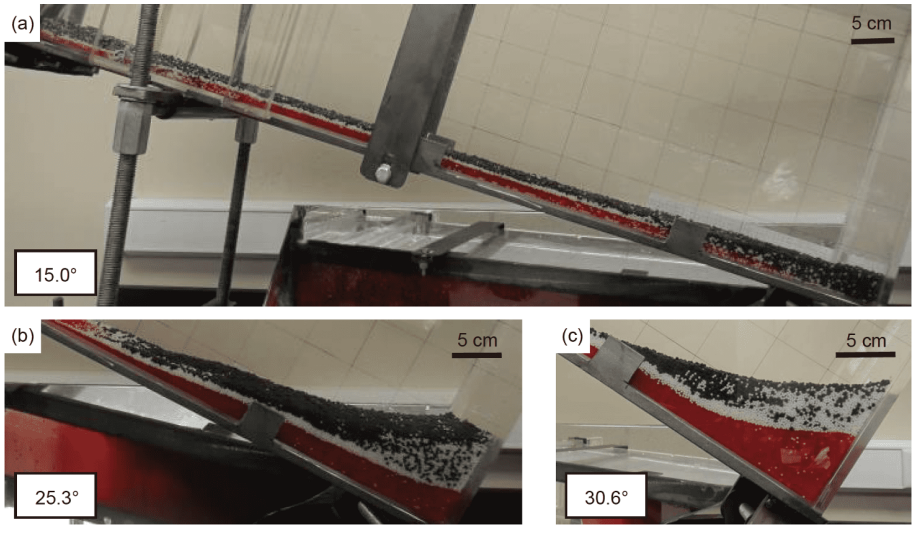

Figure 14 Analogue experiments mimicking the sorting and segregation of particles with various densities in the flowing viscous fluid (modified after Forien et al., 2015). Three inclination angles were applied during the experiments. Red glass beads (2.52 g cm^{-3}), white polyacetal balls (1.41 g cm^{-3}), and black silicone balls (1.30 g cm^{-3}) are used to simulate chromite, pyroxene, and plagioclase in nature melt. Glycerine with a density of 1.26 g cm^{-3} and viscosity of 1.41 Pa s was used to represent the silicate liquid.

5.4.2 Damiao-type high-grade iron deposits

Fe-Ti-P-rich ore dikes/veins beneath the Damiao massif-type anorthosite complex occur as discordant late-stage dikes cross-cutting early-stage anorthosites with irregular but sharp boundaries, which represent the evolved products of residual magma due to the residual Fe-rich magma after the segregation of early-stage anorthosites (Zhao et al., 2009; Li L X et al., 2019b). However, the mechanism by which iron was highly concentrated during the evolution of magma are currently highly contentious, with both liquid immiscibility and fractional crystallization models proposed. Some researchers believe that gabbronorites were solidification product of residual melts, which could also develop liquid immiscibility to separate into Fe-rich and Si-rich magmas. Subsequently, Fe-rich melt could crystallize to form Fe-rich veins/dikes and Si-rich magma lead eventually to the formation of granitic dikes (e.g., Chen et al., 2013; He et al., 2016). Other researchers suggest that progressive and extensive fractional crystallization is probably responsible for the formation of large-scale massive Fe-Ti-P-rich silicate rocks and Fe-Ti-P-rich ores (Li L X et al., 2015). Nevertheless, both mechanisms cannot explain the formation of Fe-Ti oxide-apatite (nelsonite) without presence of any silicate minerals. Experiments had shown that the near pure Fe-Ti-P ore magma (nelsonitic in composition) cannot exist under natural conditions with the liquid immiscibility mechanism (Wang M et al., 2017). With respect to the fractional crystallization mechanism, it is hard to explain the fully separation of apatite from clinopyroxene (~3.5 g cm^{-3}) with similar density, and also the co-existence of both apatite and magnetite which are quite different in density, and the vein/dike-shaped occurrence of ore bodies (e.g., Zhao et al., 2010; Zhang, 2018).

Extensive alteration in the Damiao-type Fe-Ti-P-rich ore veins indicate that the activities of hydrothermal fluid is closely related to the mineralization. Apatite in the high-grade iron ore contains abundant primary fluid inclusions and microthermometric studies demonstrate fluids associated with mineralization is in the system $CaCl_2$-NaCl-H_2O-CO_2 (Li et al., 2010). Vermiculite and/or chlorite-hosted melt inclusions in apatite indicate that there are more fluids in Fe-Ti-P-rich magma during late-stage melt evolution (Wang M et al., 2017). The petrogenetic mineralogy and volatile composition of zircon in the Fe-Ti-P-rich ores show that the increasing of H_2O and CO_2 contents in the late-stage of Fe-Ti-P-rich magma evolution led to increase of oxygen fugacity in the magma, and finally the crystallization of magnetite (Xing et al., 2011; Zhou J L et al., 2013). It is worth noting that the Damiao-type Fe-Ti-P-rich veins/dikes mainly exist in the altered white-colored anorthosite, while almost no ore bodies occurred in the fresh dark-colored anorthosite. Petrographic observation shows that plagioclase is a common mineral in the dark-colored anorthosite and occurs in association with abundant rod-shaped Fe-Ti oxides exsolution, while no inclusion occurs in the white-colored anorthosite. During the alteration of dark-colored anorthosite, Fe was leached and transported by hydrothermal fluids, and its precipitation along the pre-existing fractures of the anorthosite resulted in the formation of massive Fe-Ti-P orebodies (Li H M et al., 2014a). Li L X et al. (2019c) also supported the hypothesis, as baddeleyite-zircon relationships in unaltered anorthosite, altered anorthosite and Fe-rich ore indicate that the metallogenic fluid phase exsolved from magma at a temperature higher than ~700°C, and the hydrothermal fluid flow was still active at ~350°C. It is also suggested that the Fe-Ti-P mineralization of the Damiao anorthosite complex was associated with magmatic-hydrothermal processes, with the Fe-Ti oxides being formed at the magmatic stage and apatite precipitated throughout the magmatic-hydrothermal stages.

5.5 Genetic mechanism and key control factors of high-grade iron deposits

5.5.1 Iron ore magma and high-grade iron ore

As mentioned above, there is always sharp contact between massive ore and wall rocks in magmatic, volcanic-hosted (including both continental and submarine) or skarn high-grade iron deposits. Therefore, some studies suggested that high-grade iron ores may be attributed to the direct injection and condensation of Fe(-P) ore magma formed by liquid immiscibility (e.g., Buddington et al., 1955; Zhou et al., 2005; Tornos et al., 2016). However, experimental studies show that high temperature magmas could develop liquid immiscibility to produce Fe-rich silicate melt but hard to form pure oxide ore magma (Philpotts, 1981, 1982). Therefore, many researchers believed that there is no pure oxide ore magma in nature (e.g., Lindsley and Epler, 2017; Wang M et al., 2017). Thus, the relationship between magmatic massive ore and pure oxide ore magma has been debated for decades.

Recently, Hou et al. (2018) obtained Fe-P melt and Fe-Ca-P melt produced by immiscibility experiment under hydrous and oxidized condition (FMQ+3.1–+3.3), as well as silica-rich rhyolitic melts. Moreover, Xie et al. (2019) found melt inclusions (Fe-P melts and rhyolitic melts) with similar composition to immiscibility experimental results in El Laco iron deposits, Chile. However, the experimental results are also different from massive ores, i.e., there are a small amount of SiO_2, MgO and CaO in the immiscible melt of massive ore, which indicates that massive ores were formed as a result of later further reworking, rather than direct condensation. Additionally, the magnetite in the immiscibility experiment is reasonably enriched in Ti, while the ores from volcanic-hosted (including both continental and submarine) and skarn-type high-grade iron deposit is mostly low-Ti magnetite. Therefore, it is unlikely

that the volcanic-hosted and skarn-type high-grade iron deposits are formed by direct crystallization of pure oxide ore magma. Similarly, liquid immiscibility may play an important role in the formation of Damiao anorthosite-type Fe-Ca-P-rich ores, but the rocks had also been altered and re-worked by fractional crystallization and hydrothermal fluid activities.

5.5.2 Metallogenic mechanism of the high-grade iron deposits: multi-stage/phase superimposition and reworking

Based on the discussion above, the metallogenic mechanism of skarn, sedimentary metamorphic, volcanic-hosted and magmatic high-grade iron deposits are not formed by a single ore-forming process, but by multi-stage superimposition and reworking. There are two types in the aspect of temporal evolution: (1) Temporally continuous mineralization type, or multi-stage superimposition type. Mineralization was developed continuously by multi-stage superimposition of Fe-rich magma/ore-forming fluid driven by same magmatic heat source or same tectonic stress. The mineralization type is similar, and multi-stages are genetically related to each other. Such type of mineralization includes magmatic (e.g., Panzhihua-type and Damiao-type), skarn, volcanic-hosted (including both continental and submarine) high-grade iron deposits; (2) temporally discontinuous mineralization, or multi-episode superimposition type. It refers to the deposits formed by multi-episode superimposition with completely different types of metallogenic processes, obvious difference in mineralization ages and different phases lack genetic correlation among mineralization phases. Typical example is the sedimentary metamorphic type, including Shilu and #2 ore section in Gongchangling.

The formation of multi-stage superimposition-type high-grade iron deposits are generally divided into three stages: (1) Mineralization occurred during magmatic stage, e.g., Panzhihua-type, in which fractional crystallization plays an important role, and high-density magnetite could be further enriched due to flow differentiation; (2) mineralization occurred during magmatic-hydrothermal transition stage, e.g., Damiao-type deposit. The high-grade iron ores are mostly formed during this stage; and (3) mineralization occurred during the hydrothermal stage, such as skarn and volcanic-hosted (including both continental and submarine) high-grade iron deposits. Mineralization involves both magmatic and hydrothermal stages, i.e., the exsolution of Fe-rich fluid with high temperature and high salinity during magmatic stage is important for the final product, i.e., high-grade iron ores. However, the key processes for the formation of them happened during the hydrothermal stage, requiring a combination of removal of impurity components, and re-mobilization and re-precipitation of iron via multi-stage hydrothermal superimposition and reworking.

6. Conclusions

(1) Geological settings of various types of high-grade iron deposits in China are summarized as follows: BIFs formed by global oxygen-deficient environment during late Archean, and iron had been enriched under shallow marine environment in the redox-stratified ocean. Extensive development of both skarn and continental volcanic-hosted iron deposits in Eastern China were genetically associated with the rapid extension and thinning of sub-continental lithospheric mantle. The interaction between mantle plume and sub-continental lithospheric mantle containing eclogitic materials which were formed by ancient subduction is the key factor controlling the formation of giant Fe-Ti-V oxide deposits. High-angle subduction under hot mantle-cold crust circumstance is the most favorable condition for the formation of submarine volcanic iron deposits.

(2) High-grade massive iron ores related to magmatism were not formed by solidification of oxide melt (ore magma) but by multiple-stage superimposition and reworking in the magmatic-hydrothermal system.

(3) The formation of various high-grade iron deposits was also coupled by removal of silica and other impurity, and remobilization and re-precipitation of iron via multiple-stage superimposition and reworking. According to the temporal evolution consequences, the high-grade iron deposits could be divided into multi-episode superimposition type and multi-stage superimposition type. Therefore, the formation of sedimentary metamorphic type iron deposits predominantly is attributed to multi-episode reworking, and other types including skarn, volcanic-hosted and magmatic types related to magmatic-hydrothermal fluids belong to the multi-stage superimposition type.

Acknowledgements *Special thanks to the critical and constructive reviews by three anonymous experts, which significantly improved the quality of the manuscript. Due to the length limitation, we are sorry for not being able to cite all the relevant studies in literature. This work was supported by the National Basic Research Program of China (Grant No. 2012CB416800).*

References

Bai Z J, Zhong H, Li C S, Zhu W G, He D F, Qi L. 2014. Contrasting parental magma compositions for the Hongge and Panzhihua magmatic Fe-Ti-V oxide deposits, Emeishan large igneous province, SW China. Econ Geol, 109: 1763–1785

Bai Z J, Zhong H, Naldrett A J, Zhu W G, Xu G W. 2013. Whole-rock and mineral composition constraints on the genesis of the giant Hongge Fe-Ti-V oxide deposit in the Emeishan Large Igneous Province, Southwest China. Econ Geol, 107: 507–524

Basta F F, Maurice A E, Fontboté L, Favarger P Y. 2011. Petrology and geochemistry of the banded iron formation (BIF) of Wadi Karim and Um Anab, Eastern Desert, Egypt: Implications for the origin of Neoproterozoic BIF. Precambrian Res, 187: 277–292

Bekker A, Slack J F, Planavsky N, Krapez B, Hofmann A, Konhauser K O, Rouxel O J. 2010. Iron formation: The sedimentary product of a complex interplay among mantle, tectonic, oceanic, and biospheric

processes. Econ Geol, 105: 467–508
Buddington A F, Fahey J J, Vlisidis A C. 1955. Thermometric and petrogenetic significance of titaniferous magnetite. Am J Sci, 253: 497–532
Cao Y, Wang C Y, Huang F, Zhang Z. 2019. Iron isotope systematics of the Panzhihua mafic layered intrusion associated with giant Fe-Ti oxide deposit in the Emeishan large igneous province, SW China. J Geophys Res Solid Earth, 124: 358–375
Chang Y F, Li J H, Song C Z. 2019. The regional tectonic framework and some new understandings of the Middle-Lower Yangtze River Valley Metallogenic Belt (in Chinese). Acta Petrol Sin, 35: 3579–3591
Chang Y F, Liu P X, Wu Y C. 1991. The Copper-Iron Belt of the Lower and Middle Reaches of the Changjiang River (in Chinese). Beijing: Geological Publishing House. 1–380
Chang Z S, Shu Q H, Meinert L. 2019. Skarn deposits of China. In: Chang Z S, Goldfarb R J, eds. Mineral Deposits of China. Lawrence: Society of Economic Geologists. 189–234
Chen B, Tian W, Jahn B M, Chen Z C. 2008. Zircon SHRIMP U-Pb ages and in-situ Hf isotopic analysis for the Mesozoic intrusions in South Taihang, North China craton: Evidence for hybridization between mantle-derived magmas and crustal components. Lithos, 102: 118–137
Chen B, Zhai M G, Tian W. 2007. Origin of the Mesozoic magmatism in the North China Craton: Constraints from petrological and geochemical data. Geol Soc Lond Spec Publ, 280: 131–151
Chen L C, Liu D Q, Tang Y L, Wang D H, Dong L H, Xu X, Wang X D. 2008. Mineral Resources and Producing Places in Tianshan of China (Part I) (in Chinese). Beijing: Geological Publishing House. 243–287
Chen W T, Zhou M F, Zhao T P. 2013. Differentiation of nelsonitic magmas in the formation of the ~1.74 Ga Damiao Fe-Ti-P ore deposit, North China. Contrib Mineral Petrol, 165: 1341–1362
Chen Z L, Chen B L, Li H M, Du W H, Li L X, Han F B, Wang Y, Sun Y, Wu Y, Zhang W G. 2014. Geological characteristic of the Damiao iron deposit, North China Craton and ore-prospecting (in Chinese). Acta Geol Sin, 88: 2339–2350
Chen Z L, Ding W J, Cui L Contra, Chen B L, Han F B, Zhou Y G, Dong F X, Yang N. 2010. High-grade large iron ore deposit and its formation prospecting of Xing Shan, Xian An, Hebei Province (in Chinese). Miner Depos, 29: 71–72
Deng X D, Li J W, Luo T, Wang H Q. 2017. Dating magmatic and hydrothermal processes using andradite-rich garnet U-Pb geochronometry. Contrib Mineral Petrol, 172: 71
Deng X D, Li J W, Wen G. 2014. Dating iron skarn mineralization using hydrothermal allanite-(La) U-Th-Pb isotopes by laser ablation ICP-MS. Chem Geol, 382: 95–110
Deng X D, Li J W, Wen G. 2015. U-Pb geochronology of hydrothermal zircons from the early Cretaceous iron skarn deposits in the Handan-Xingtai district, North China craton. Econ Geol, 110: 2159–2180
Dill H G. 2010. The "Chessboard" classification scheme of mineral deposits: Mineralogy and geology from aluminum to zirconium. Earth-Sci Rev, 100: 1–420
Duan S G, Zhang Z H, Jiang Z S, Zhao J, Zhang Y, Li F, Tian J. 2014. Geology, geochemistry, and geochronology of the Dunde iron-zinc ore deposit in western Tianshan, China. Ore Geol Rev, 57: 441–461
Duchesne J C, Liegeois J P, Vander Auwera J, Longhi J. 1999. The crustal tongue melting model and the origin of massive anorthosites. Terra Nova, 11: 100–105
Fan Y, Zhou T F, Yuan F, Tang M H, Zhang L J, Ma L, Xie J. 2010. High sulfidation epithermal hydrothermal system in Lu-Zong volcanic basin, Evidence from geological characteristics and sulfur isotope data of Fanshan alunite deposit (in Chinese). Acta Petrol Sin, 26: 3657–3666
Forien M, Tremblay J, Barnes S J, Burgisser A, Pagé P. 2015. The role of viscous particle segregation in forming chromite layers from slumped crystal slurries: Insights from analogue experiments. J Petrol, 56: 2425–2444
Hagemann S G, Angerer T, Duuring P, Rosière C A, Figueiredo e Silva R C, Lobato L, Hensler A S, Walde D H G. 2016. BIF-hosted iron mineral system: A review. Ore Geol Rev, 76: 317–359
He H L, Yu S Y, Song X Y, Du Z S, Dai Z H, Zhou T, Xie W. 2016. Origin of nelsonite and Fe-Ti oxides ore of the Damiao anorthosite complex, NE China: Evidence from trace element geochemistry of apatite, plagioclase, magnetite and ilmenite. Ore Geol Rev, 79: 367–381
He Y. 2007. The geological and geochemical feature of iron deposit of Yamansu, Hami (in Chinese). West-China Exp Eng, 11: 142–144
Henríquez F, Martin R. 1978. Crystal-growth textures in magnetite flows and feeder dykes, El Laco, Chile. Can Mineral, 16: 581–589
Henríquez F, Nyström J O. 1998. Magnetite bombs at El Laco volcano, Chile. GFF, 120: 269–271
Hildebrand R S. 1986. Kiruna-type deposits; their origin and relationship to intermediate subvolcanic plutons in the Great Bear magmatic zone, Northwest Canada. Econ Geol, 81: 640–659
Hou T, Charlier B, Holtz F, Veksler I, Zhang Z, Thomas R, Namur O. 2018. Immiscible hydrous Fe-Ca-P melt and the origin of iron oxide-apatite ore deposits. Nat Commun, 9: 1415
Hou T, Zhang Z C, Du Y S, Li S T. 2009. Geology of the Gushan iron oxide deposit associated with dioritic porphyries, eastern Yangtze craton, SE China. Int Geol Rev, 51: 520–541
Hou T, Zhang Z C, Encarnacion J, Santosh M, Sun Y L. 2013. The role of recycled oceanic crust in magmatism and metallogeny: Os-Sr-Nd isotopes, U-Pb geochronology and geochemistry of picritic dykes in the Panzhihua giant Fe-Ti oxide deposit, central Emeishan large igneous province, SW China. Contrib Mineral Petrol, 165: 805–822
Hou T, Zhang Z C, Ye X R, Encarnacion J, Reichow M K. 2011. Noble gas isotopic systematics of Fe-Ti-V oxide ore-related mafic-ultramafic layered intrusions in the Panxi area, China: The role of recycled oceanic crust in their petrogenesis. Geochim Cosmochim Acta, 75: 6727–6741
Hu H, Lentz D R, Li J W, McCarron T, Zhao X F, Hall D. 2015. Re-equilibration processes in magnetite from iron skarn deposits. Econ Geol, 110: 1–8
Hu H, Li J W, Harlov D E, Lentz D R, McFarlane C R M, Yang Y H. 2020. A genetic link between iron oxide-apatite and iron skarn mineralization in the Jinniu volcanic basin, Daye district, eastern China: Evidence from magnetite geochemistry and multi-mineral U-Pb geochronology. GSA Bull, 132: 899–917
Hu H, Li J W, Lentz D, Ren Z, Zhao X F, Deng X D, Hall D. 2014a. Dissolution-reprecipitation process of magnetite from the Chengchao iron deposit: Insights into ore genesis and implication for in-situ chemical analysis of magnetite. Ore Geol Rev, 57: 393–405
Hu H, Duan Z, Luo Y, Li J W. 2014b. Trace element systematics of magnetite from the Chengchao iron deposit in the Daye district: A laser ablation ICP-MS study and insights into ore genesis (in Chinese). Acta Petrol Sin, 30: 1292–1306
Hu X, Chen H Y, Zhao L D, Han J S, Xia X P. 2017. Magnetite geochemistry of the Longqiao and Tieshan Fe-(Cu) deposits in the Middle-Lower Yangtze River Belt: Implications for deposit type and ore genesis. Ore Geol Rev, 89: 822–835
Huang Q T, Yin G P. 1989. The Luohe Iron Deposit in Lujiang County, Anhui Province (in Chinese). Beijing: Geological Publishing House. 1–193
Isley A E. 1995. Hydrothermal plumes and the delivery of iron to banded iron-formation. J Petrol, 103: 169–185
Jiang Z S, Zhang Z H, Wang Z H, Duan S G, Li F M, Tian J Q. 2014. Geology, geochemistry, and geochronology of the Zhibo iron deposit in the Western Tianshan, NW China: Constraints on metallogenesis and tectonic setting. Ore Geol Rev, 57: 406–424
Jiang Z S, Zhang Z H, Hou K J, Hong W, Wang Z H, Li F M and Tian J Q. 2012. Geochemistry and zircon U-Pb age of volcanic rocks from the Chagangnuoer and Zhibo iron deposits, western Tianshan, and their geological significance (in Chinese). Acta Petrol Sin, 28: 2074–2088
Jiang Z S. 2014. Carboniferous volcanism and Fe mineralization at the Zhibo iron deposit in the western Tianshan (in Chinese). Dissertation for Doctoral Degree. Beijing: Chinese Academy of Geological Sciences
Klein C. 2005. Some Precambrian banded iron-formations (BIFs) from around the world: Their age, geologic setting, mineralogy, metamorphism, geochemistry, and origins. Am Miner, 90: 1473–1499

Konhauser K O, Planavsky N J, Hardisty D S, Robbins L J, Warchola T J, Haugaard R, Lalonde S V, Partin C A, Oonk P B H, Tsikos H, Lyons T W, Bekker A, Johnson C M. 2017. Iron formations: A global record of Neoarchaean to Palaeoproterozoic environmental history. Earth-Sci Rev, 172: 140–177

Lester G W, Clark A H, Kyser T K, Naslund H R. 2013. Experiments on liquid immiscibility in silicate melts with H_2O, P, S, F and Cl: Implications for natural magmas. Contrib Mineral Petrol, 166: 329–349

Li H M, Ding J H, Zhang Z C, Li L X, Chen J, Yao T. 2015b. Iron-rich fragments in the Yamansu iron deposit, Xinjiang, NW China: Constraints on metallogenesis. J Asian Earth Sci, 113: 1068–1081

Li H M, Li L X, Ding J H, Li Y H, Song Z, Meng J, Ma Y B. 2018. Occurrence of the iron-rich melt in the Heijianshan iorn deposit, Eastern Tianshan, NW China: Insights into the origin of volcanic rock-hosted iron deposits. Acta Geol Sin-Engl Ed, 92: 666–681

Li H M, Li L X, Zhang Z C, Santosh M, Liu M J, Cui Y H, Yang X Q, Chen J, Yao T. 2014a. Alteration of the Damiao anorthosite complex in the northern North China Craton: Implications for high-grade iron mineralization. Ore Geol Rev, 57: 574–588

Li H M, Liu M J, Li L X, Yang X Q, Yao L D, Chen J, Yao T. 2014b. SHRIMP U-Pb geochronology of zircons from the garnet-rich altered rocks in the mining area II of the Gongchangling iron deposit: Constraints on the ages of the high-grade iron deposit (in Chinese). Acta Petrol Sin, 30: 1205–1217

Li H M, Wang D H, Li L X, Chen J, Yang X Q, Liu M J. 2012. Metallogeny of iron deposits and resource potential of major iron minerogenetic units in China (in Chinese). Geol China, 39: 559–580

Li H M, Yang X Q, Li L X, Zhang Z C, Liu M J, Yao T, Chen J. 2015a. Desilicification and iron activation-reprecipitation in the high-grade magnetite ores in BIFs of the Anshan-Benxi area, China: Evidence from geology, geochemistry and stable isotopic characteristics. J Asian Earth Sci, 113: 998–1016

Li J L, Zhang G L, Su L H. 1986. An experimental study on the iron ore deposits formed by "ore magma" related to FeO-$Ca_5(PO_4)_3F$-$NaAlSiO_4$-$CaMgSi_2O_6$ system (in Chinese). Bull Instit Mineral Deposits Chin Acad Geol Sci, 18: 197–204

Li J W, Vasconcelos P M, Zhou M F, Deng X D, Cohen B, Bi S J, Zhao X F, Selby D. 2014. Longevity of magmatic-hydrothermal systems in the Daye Cu-Fe-Au District, eastern China with implications for mineral exploration. Ore Geol Rev, 57: 375–392

Li J W, Zhao X F, Deng X D, Tan J, Hu H, Zhang D Y, Li Z K, Li H, Rong H, Yang M Z, Cao K, Jin X Y, Sui J X, Zu B, Chang J, Wu Y F, Wen G, Zhao S R. 2019. An overview of the advance on the study of China's ore deposits during the last seventy years (in Chinese). Sci Sin Terr, 49: 1720–1771

Li J W, Zhao X F, Zhou M F, Ma C Q, de Souza Z S, Vasconcelos P. 2009. Late Mesozoic magmatism from the Daye region, eastern China: U-Pb ages, petrogenesis, and geodynamic implications. Contrib Mineral Petrol, 157: 383–409

Li L X, Li H M, Li Y Z, Yao T, Yang X Q, Chen J. 2015. Origin of rhythmic anorthositic-pyroxenitic layering in the Damiao anorthosite complex, China: Implications for late-stage fractional crystallization and genesis of Fe-Ti oxide ores. J Asian Earth Sci, 113: 1035–1055

Li L X, Li H M, Chen Z L, Wang D H, Chen W S. 2010. Hydrothermal mineralization and fluid inclusion study on the Heishan iron deposit, Chengde County, Hebei Province, China (in Chinese). Acta Petrol Sin, 26: 858–870

Li L X, Li H M, Zi J W, Rasmussen B, Sheppard S, Ma Y B, Meng J, Song Z. 2019a. The link between an anorthosite complex and underlying olivine–Ti-magnetite-rich layered intrusion in Damiao, China: Insights into magma chamber processes in the formation of Proterozoic massif-type anorthosites. Contrib Mineral Petrol, 174: 48

Li L X, Li H M, Zi J W, Rasmussen B, Sheppard S, Wilde S A, Meng J. 2019b. Role of fluids in Fe-Ti-P mineralization of the Proterozoic Damiao anorthosite complex, China: Insights from baddeleyite-zircon relationships in ore and altered anorthosite. Ore Geol Rev, 115: 103186

Li L X, Zi J W, Li H M, Rasmussen B, Wilde S A, Sheppard S, Ma Y B, Meng J, Song Z. 2019c. High-grade magnetite mineralization at 1.86 Ga in Neoarchean banded iron formations, Gongchangling, China: *In situ* U-Pb geochronology of metamorphic-hydrothermal zircon and monazite. Econ Geol, 114: 1159–1175

Li L X, Zi J W, Meng J, Li H M, Rasmussen B, Sheppard S, Wilde S A, Li Y H. 2020. Using *in situ* monazite and xenotime U-Pb geochronology to resolve the fate of the "missing" banded iron formation-hosted high-grade hematite ores of the North China Craton. Econ Geol, 115: 189–204

Li N B, Niu H C, Zhang X C, Zeng Q S, Shan Q, Li C Y, Yan S, Yang W B. 2015. Age, petrogenesis and tectonic significance of the ferrobasalts in the Chagangnuoer iron deposit, western Tianshan. Int Geol Rev, 57: 1218–1238

Li W, Xie G, Mao J, Zhu Q, Zheng J. 2019. Mineralogy, fluid inclusion, and stable isotope studies of the Chengchao deposit, Hubei province, eastern China: Implications for the formation of high-grade Fe skarn deposits. Econ Geol, 114: 325–352

Li Y H, Xie G Q, Duan C, Han D, Wang C Y. 2013. Effect of sulfate evaporate salt layer over the formation of skarn-type iron ores (in Chinese). Acta Petrol Sin, 87: 1324–1333

Li Y H, Zhang Z J, Hou K J, Duan C, Wang D H, Hu G Y. 2014. The genesis of Gongchangling high-grade-iron ores, Anshan-Benxi area, Liaoning Province, NE China: Evidence from Fe-Si-O-S isotopes (in Chinese). Acta Geol Sin, 88: 2351–2372

Li Z H, Zhu X K, Sun J. 2014. Geochemical characteristics of Banded Iron-Formations from Xinyu and North China (in Chinese). Acta Petrol Sin, 30: 1279–1291

Lindsley D H, Epler N. 2017. Do Fe-Ti-oxide magmas exist? Probably not! Am Miner, 102: 2157–2169

Liu P P, Zhou M F, Chen W T, Boone M, Cnudde V. 2014. Using multiphase solid inclusions to constrain the origin of the Baima Fe-Ti-(V) Oxide deposit, SW China. J Petrol, 55: 951–976

Liu Y N, Fan Y, Zhou T F, Xiao X, White N C, Thompson J, Hong H L, Zhang L J. 2019. Geochemical characteristics of magnetite in Longqiao skarn iron deposit in the Middle-Lower Yangtze Metallogenic Belt, Eastern China. Miner Depos, 54: 1229–1242

Lu D R, Ji J S, Lu R S, Tao H X. 1995. Geochemical characteristics of the rare earth elements of the Yamansu iron deposit (in Chinese). J Xi'an College Geol, 18: 12–16

Mao J W, Xie G Q, Duan C, Pirajno F, Ishiyama D, Chen Y C. 2011. A tectono-genetic model for porphyry-skarn-stratabound Cu-Au-Mo-Fe and magnetite-apatite deposits along the Middle-Lower Yangtze River Valley, Eastern China. Ore Geol Rev, 43: 294–314

Meinert L D, Dopple G M, Nicolescu S. 2005. World skarn deposits. In: Hedenquist J W, et al., eds. Economic Geology 100th Anniversity Volume. Littleleton: Society of Economic Geologists. 299–336

Morris RC. 1983. Supergene alteration of banded iron formation. In: Trendall A F, Morris R C, eds. Iron Formation: Facts and Problems. Amsterdam: Elsevier Science Publications. 513–534

Naslund H R. 1983. The effect of oxygen fugacity on liquid immiscibility in iron-bearing silicate melts. Am J Sci, 283: 1034–1059

Naslund H R, Henriquez F, Nyström J O, Vivallo W, Dobbs F M. 2002. Magmatic iron ores and associated mineralisation: Examples from the Chilean High Andes and Coastal Cordillera. In: Porter T M, ed. Hydrothermal iron oxide copper-gold and related deposits: A global perspective. Adelaide: PGC Publishing. 207–226

Nyström J O, Henriquez F. 1994. Magmatic features of iron ores of the Kiruna type in Chile and Sweden: Ore textures and magnetite geochemistry. Econ Geol, 89: 820–839

Pang K N, Zhou M F, Lindsley D, Zhao D, Malpas J. 2008. Origin of Fe-Ti oxide ores in mafic intrusions: Evidence from the Panzhihua Intrusion, SW China. J Petrol, 49: 295–313

Park C F. 1961. A magnetite "Flow" in northern Chile. Econ Geol, 56: 431–436

Philpotts A R. 1967. Origin of certain iron-titanium oxide and apatite rocks. Econ Geol, 62: 303–315

Philpotts A R. 1981. A model for the generation of massif-type anortho-

sites. Can Mineral, 19: 233–253
Philpotts A R. 1982. Compositions of immiscible liquids in volcanic rocks. Contr Mineral Petrol, 80: 201–218
Pokrovski G S, Dubrovinsky L S. 2011. The S^{3-} ion is stable in geological fluids at elevated temperatures and pressures. Science, 331: 1052–1054
Research Group of Ningwu. 1978. Ningwu Porphyrite Iron Ore (in Chinese). Beijing: Geological Publishing House. 1–196
Shen Q H, Song H X. 2015. Progress, prospecting and key scientific problems in origin researches of high-grade iron ore of the banded iron-formation (BIF) in the North China Craton (in Chinese), Acta Petrol Sin, 31: 2795–2815
Shu Q A, Chen P L, Cheng J R. 1992. The Geology of Iron and Copper Deposits in Eastern Hubei Province, China (in Chinese). Beijing: Metallurgical Industry Press Co., Ltd. 1–532
Sillitoe R H, Burrows D. 2002. New field evidence bearing on the origin of the El Laco magnetite deposit, northern Chile. Econ Geol, 97: 1101–1109
Song X Y, Qi H W, Hu R Z, Chen L M, Yu S Y, Zhang J F. 2013. Formation of thick stratiform Fe-Ti oxide layers in layered intrusion and frequent replenishment of fractionated mafic magma: Evidence from the Panzhihua intrusion, SW China. Geochem Geophys Geosyst, 14: 712–732
Song X Goosy, Chen Y C, Sheng J F, Ai Y D. 1981. On iron deposit formed from volcanic-hypabyssal ore magma (in Chinese). Acta Geol Sin, 1: 43-86
Sun J, Luo Z H, Zhang C H, Guo S F, Li J, Du W H, Wang D Z, Pan Y, Zhou J L, Li X D. 2009. Is the Damiao ore field a crisis mine or a potential giant iron base? (in Chinese). Geol China, 36: 255–267
Sun W D, Ling M X, Wang F Y, Ding X, Hu Y H, Zhou J B, Yang X Y. 2008. Pacific plate subduction and Mesozoic geological event in Eastern China (in Chinese). Bull Miner Petrol Geochem 27: 218–225
Sun X H, Tang H S, Luan Y, Chen J H. 2020. Geochronological constraints on the genesis of high-grade iron ore in the Gongchangling BIFs from the Anshan-Benxi area, North China Craton. Ore Geol Rev, 122: 103504
Tornos F, Velasco F, Hanchar J M. 2016. Iron-rich melts, magmatic magnetite, and superheated hydrothermal systems: The El Laco deposit, Chile. Geology, 44: 427–430
Tornos F, Velasco F, Hanchar J M. 2017. The magmatic to magmatic-hydrothermal evolution of the El Laco deposit (Chile) and its implications for the genesis of magnetite-apatite deposits. Econ Geol, 112: 1595–1628
Tuff J, Takahashi E, Gibson S A. 2005. Experimental constraints on the role of garnet pyroxenite in the genesis of high-Fe mantle plume derived melts. J Petrol, 46: 2023–2058
Vander Auwera J, Bolle O, Bingen B, Liégeois J P, Bogaerts M, Duchesne J C, De Waele B, Longhi J. 2011. Sveconorwegian massif-type anorthosites and related granitoids result from post-collisional melting of a continental arc root. Earth-Sci Rev, 107: 375–397
VIDRGMLCJV (Volcanic Iron Deposit Research Group of the Middle-Lower Yangtze Valley). 1977. Porphyrite iron ore—A genetic model of a group of iron deposits in Andesitic volcanic area (in Chinese). Acta Geol Sin, 51: 1–18
Wang E D, Xia J M, Zhao C F, Fu J F, Hou G Q. 2012. Forming mechanism of high-grade magnetite bodies in Gongchangling, Liaoning Province (in Chinese). Acta Geol Sin, 86: 1761–1772
Wang D H, Li C J, Chen S P, Xiao K Y, Li H Q, Liang T. 2006. Metallogenic characteristics and direction in mineral search in the East Tianshan, Xinjiang, China (in Chinese). Geol Bull China, 25: 910–915
Wang K, Wang C Y, Ren Z Y. 2018. Apatite-hosted melt inclusions from the Panzhihua gabbroic-layered intrusion associated with a giant Fe-Ti oxide deposit in SW China: Insights for magma unmixing within a crystal mush. Contrib Mineral Petrol, 173: 59
Wang M, Veksler I, Zhang Z, Hou T, Keiding J K. 2017. The origin of nelsonite constrained by melting experiment and melt inclusions in apatite: The Damiao anorthosite complex, North China Craton. Gondwana Res, 42: 163–176
Wang W, Chai F M, Wang H P, Yang J J, Li Q, Gu G L. 2017. Inclusions study of Jibote iron deposit in the Chinese Altay orogenic belt: Evidence of magmatic in origin (in Chinese). Chinese J Geol, 52: 571–591
Wang X S, Zhang X, Gao J, Li J L, Jiang T, Xue S C. 2018. A slab break-off model for the submarine volcanic-hosted iron mineralization in the Chinese Western Tianshan: Insights from Paleozoic subduction-related to post-collisional magmatism. Ore Geol Rev, 92: 144–160
Wang Z, Xu D, Hu G, Yu L, Wu C, Zhang Z, Cai J, Shan Q, Hou M, Chen H. 2015. Detrital zircon U-Pb ages of the Proterozoic metaclastic-sedimentary rocks in Hainan Province of South China: New constraints on the depositional time, source area, and tectonic setting of the Shilu Fe-Co-Cu ore district. J Asian Earth Sci, 113: 1143–1161
Wang Z L, Xu D R, Monika A K, Wu C J, Yu L L. 2015. Genesis of and CHIME dating on monazite in the Shilu iron ore deposit, Hainan Province of South China, and its geological implications (in Chinese). Acta Petrol Sin, 31: 200–216
Wen G, Bi S J, Li J W. 2017. Role of evaporitic sulfates in iron skarn mineralization: A fluid inclusion and sulfur isotope study from the Xishimen deposit, Handan-Xingtai district, North China Craton. Miner Depos, 52: 495–514
Whitney J A, Hemley J J, Simon F O. 1985. The concentration of iron in chloride solutions equilibrated with synthetic granitic compositions: The sulfur-free system. Econ Geol, 80: 444–460
Wilson R E, Harding T P, Seely D R. 1973. Basic wrench tectonics. AAPG Bull, 57: 74–96
Xie G Q, Mao J W, Zhu Q Q, Yao L, Li Y H, Li W, Zhao H J. 2015. Geochemical constraints on Cu-Fe and Fe skarn deposits in the Edong district, Middle-Lower Yangtze River metallogenic belt, China. Ore Geol Rev, 64: 425–444
Xie Q H, Zhang Z C, Hou T, Cheng Z, Campos E, Wang Z C, Fei X H. 2019. New insights for the formation of Kiruna-type iron deposits by immiscible hydrous Fe-P melt and high-temperature hydrothermal processes: Evidence from El Laco deposit. Econ Geol, 114: 35–46
Xing C M, Wang C Y. 2017. Cathodoluminescence images and trace element compositions of fluorapatite from the Hongge layered intrusion in SW China: A record of prolonged crystallization and overprinted fluid metasomatism. Am Miner, 102: 1390–1401
Xing C M, Chen W, Wang C Y, Zhao T P. 2011. Volatile compositions and C-H-O isotope compositions of Proterozoic Damiao Fe-Ti-P oxide deposit in the northern margin of the North China Craton (in Chinese). Acta Petrol Sin, 27: 1500–1510
Xu D R, Kusiak M A, Wang Z, Chen H, Bakun-Czubarow N, Wu C, Konečný P, Hollings P. 2015. Microstructural observation and chemical dating on monazite from the Shilu Group, Hainan Province of South China: Implications for origin and evolution of the Shilu Fe-Co-Cu ore district. Lithos, 216-217: 158–177
Xu D R, Wang Z L, Cai J X, Wu C J, Bakun-Czubarow N, Wang L, Chen H Y, Baker M J, Kusiak M A. 2013. Geological characteristics and metallogenesis of the Shilu Fe-ore deposit in Hainan Province, South China. Ore Geol Rev, 53: 318–342
Xu D R, Wang Z L, Chen H Y, Hollings P, Jansen N H, Zhang Z C, Wu C J. 2014. Petrography and geochemistry of the Shilu Fe-Co-Cu ore district, South China: Implications for the origin of a Neoproterozoic BIF system. Ore Geol Rev, 57: 322–350
Xu D R, Xiao Y, Xia B, Cai R J, Hou W, Wang L, Liu Z L, Zhao B. 2009. Metallogenic Model and Prospecting Prediction of Shilu Iron Deposit in Hainan Province (in Chinese). Beijing: Geological Publishing House. 1–331
Xu Y, Chung S L, Jahn B, Wu G. 2001. Petrologic and geochemical constraints on the petrogenesis of Permian-Triassic Emeishan flood basalts in southwestern China. Lithos, 58: 145–168
Yang F Q, Mao J W, Liu F, Chai F M, Geng X X, Zhang Z X, Guo X J, Liu G R. 2013. A review of the geological characteristics and mineralization history of iron deposits in the Altay orogenic belt of the Xinjiang, Northwest China. Ore Geol Rev, 54: 1–16
Yang X Q, Li H M, Li L X, Ma Y B, Chen J, Liu M J, Yao T, Chen W S, Yao L D. 2014. Characteristics of fluid inclusions, S, H and O isotope of

iron deposit in Anshan-Benxi area, Liaoning Province (in Chinese). Acta Geol Sin, 88: 1917–1031
Yang Y L, Ni P, Pan J Y, Wang G G, Xu Y F. 2017. Constraints on the mineralization processes of the Makeng iron deposit, eastern China: Fluid inclusion, H-O isotope and magnetite trace element analysis. Ore Geol Rev, 88: 791–808
Yao P H. 1993. Records of China's Iron Ore Deposits (in Chinese). Beijing: Metallurgic Industry Press. 1–622
Yao S Z. 1983. A preliminary study on geological characteristics and some genetic problems of the slurry-hydrothermal transition iron ore deposit in Lingxiang, Hubei province (in Chinese). Geol Sci Tech Inf, S1: 71–78
Yu L, Zou S, Cai J, Xu D, Zou F, Wang Z, Wu C, Liu M. 2016. Geochemical and Nd isotopic constraints on provenance and depositional setting of the Shihuiding Formation in the Shilu Fe-Co-Cu ore district, Hainan Province, South China. J Asian Earth Sci, 119: 100–117
Yuan J Z. 1990. Iron ore types and genesis of Meishan iron ore deposit: The study of high temperature experiments (in Chinese). Geoscience, 4: 77–84
Zeng L P, Zhao X F, Hammerli J, Fan T W T, Spandler C. 2019. Tracking fluid sources for skarn formation using scapolite geochemistry: An example from the Jinshandian iron skarn deposit, Eastern China. Miner Depos, 55: 1029–1046
Zhai Y S, Yao S Z, Lin X D, Zhou Z R, Wan T F, Jin F J, Zhou Z G. 1992. The Ore-forming Regularity of Iron-copper (Gold) in the Middle and Lower Reaches of Yangtze River (in Chinese). Beijing: Geological Publishing House. 1–235
Zhai Y S. 1965. Rock characteristics and genesis of an anorthosite (in Chinese). Geol Rev, 23: 186–195
Zhang H W, Xie L X. 2001. New views on origin of Yamansu iron deposit in Xinjiang autonomous region (in Chinese). J Changchun Inst Tech-Nat Sci Edi, 2: 26–29
Zhang J L, Xu D R, Yu L L and Hou M Z. 2018. Zircon U-Pb dating of granite and host rock in Xinyu iron ore area, Jiangxi Province, China (in Chinese). Chin J Nonferrous Metals, 28: 971–984
Zhang L C, Zhai M G, Wan Y S, Guo J H, Dai Y P, Wang C L, Liu L. 2012b. Study of the Precambrian BIF-iron deposits in the North China Craton: Progresses and questions (in Chinese). Acta Petrol Sin, 28: 3431–3445
Zhang L C, Zhai M G, Zhang X J, Xiang P, Dai Y P, Wang C L, Pirajno F. 2012a. Formation age and tectonic setting of the Shirengou Neoarchean banded iron deposit in eastern Hebei Province: Constraints from geochemistry and SIMS zircon U-Pb dating. Precambrian Res, 222-223: 325–338
Zhang S H, Liu S W, Zhao Y, Yang J H, Song B, Liu X M. 2007. The 1.75–1.68 Ga anorthosite-mangerite-alkali granitoid-rapakivi granite suite from the northern North China Craton: Magmatism related to a Paleoproterozoic orogen. Precambrian Res, 155: 287–312
Zhang X. 2013. Study on metallogenic background and mineralization of Zhibo and Chagangnuoer iron ore deposits in West Tianshan Mountains (in Chinese). Dissertation for Doctoral Degree. Institute of Geology and Geophysics, Chinese Academy of Sciences. 1–226
Zhang Z C. 2018. Genesis of Proterozoic anorthosites and associated Fe-Ti-V-P ore deposits (in Chinese). Bull Miner Petrol Geochem, 37: 1047–1091
Zhang Z C, Hou T, Santosh M, Li H M, Li J W, Zhang Z H, Song X Y, Wang M. 2014a. Spatio-temporal distribution and tectonic settings of the major iron deposits (in Chinese): An overview. Ore Geol Rev, 57: 247–263
Zhang Z C, Mao J W, Saunders A D, Ai Y, Li Y, Zhao L. 2009. Petrogenetic modeling of three mafic-ultramafic layered intrusions in the Emeishan large igneous province, SW China, based on isotopic and bulk chemical constraints. Lithos, 113: 369–392
Zhang Z C, Santosh M, Li J W. 2015. Iron deposits in relation to magmatism in China. J Asian Earth Sci, 113: 951–956
Zhang Z C, Chai F M, Xie Q H. 2016. High-angle subduction in a thermal structure with warm mantle-cool crust: Formation of submarine volcanics-hosted iron deposits (in Chinese). Geol China, 43: 367–379
Zhang Z C, Hou T, Li H M, Li J W, Zhang Z H, Song X Y. 2014b. Enrichment mechanism of iron in magmatic hydrothermal system (in Chinese). Acta Petrol Sin, 30: 1189–1204
Zhang Z C, Mahoney J J, Mao J W, Wang F S. 2006. Geochemistry of picritic and associated basalt flows of the western Emeishan flood basalt province, China. J Petrol, 47: 1997–2019
Zhao B, Li T J. 1980. A preliminary study on the mechanism and physico-chemical conditions of formation of Gongchangling rich iron deposit (in Chinese). Geochimica, 4: 333–344
Zhao G, Wilde S A, Cawood P A, Sun M. 2001. Archean blocks and their boundaries in the North China Craton: Lithological, geochemical, structural and *P-T* path constraints and tectonic evolution. Precambrian Res, 107: 45–73
Zhao T P, Chen W, Zhou M F. 2009. Geochemical and Nd-Hf isotopic constraints on the origin of the ~1.74-Ga Damiao anorthosite complex, North China Craton. Lithos, 113: 673–690
Zhao T P, Chen W, Lu B. 2010. Characteristics and origin of Fe-Ti-P oxide deposits associated with Proterozoic massif-type anorthosite (in Chinese). Earth Sci Front, 17: 106–117
Zhao Y M, Lin W W, Bi C S, Li D S, Jiang C J. 1990. Skarn Deposit in China (in Chinese). Beijing: Geological Publishing House. 1–354
Zhao Y M, Wu L S, Bai G, Yuan Z X, Ye Q T, Huang M Z, Rui Z Y, Sheng J F, Lin W W, Deng S P, Mao J W, Bi C S, Dang Z F, Wang L S, Zhang Z H, Chen W S. 2004. Metallogeny of the Major Metallic Ore Deposits in China (in Chinese). Beijing: Geological Publishing House. 13–62
Zhao Y M. 2013. Main genetic types and geological characteristics of iron-rich ore deposits in China (in Chinese). Miner Depos, 32: 685–704
Zhao Y X. 1993. Formation Mechanism of Iron Deposit in Contact Zone in the Middle and Lower Reaches of Yangtze River (in Chinese). Wuhan: China University of Geosciences Press. 1–156
Zhou J L, Luo Z H, Pan Y, Li X D. 2013. The genesis of vein-type iron orebody occurred in magmatic iron deposit: A case study of the Heishan iron deposit, Hebei Province, China (in Chinese). Acta Petrol Sin, 29: 3555–3566
Zhou M F, Chen W T, Wang C Y, Prevec S A, Liu P P, Howarth G H. 2013. Two stages of immiscible liquid separation in the formation of Panzhihua-type Fe-Ti-V oxide deposits, SW China. Geosci Front, 4: 481–502
Zhou M F, Robinson P T, Lesher C M, Keays R R, Zhang C J, Malpas J. 2005. Geochemistry, petrogenesis and metallogenesis of the panzhihua gabbroic layered intrusion and associated Fe-Ti-V oxide deposits, Sichuan Province, SW China. J Petrol, 46: 2253–2280
Zhou M F, Yan D P, Wang C L, Qi L, Kennedy A. 2006. Subduction-related origin of the 750 Ma Xuelongbao adakitic complex (Sichuan Province, China): Implications for the tectonic setting of the giant Neoproterozoic magmatic event in South China. Earth Planet Sci Lett, 248: 286–300
Zhou S T. 1994. Banded Iron Ore Geology in Anshan-Benxi Area (in Chinese). Beijing: Geological Publishing House. 1–276
Zhou T F, Fan Y, Wang S W, White N C. 2017. Metallogenic regularity and metallogenic model of the Middle-Lower Yangtze River Valley Metallogenic Belt (in Chinese). Acta Petrol Sin, 33: 3353–3372
Zhu Q Q, Xie G Q, Li W. 2019. Superposition mechanism of Fe enrichment in skarn deposits of Edong district: Constrains from magnetite texture and ore grade data (in Chinese). Acta Petrol Sin, 35: 3703–3720
Zou S, Yu L, Yu D, Xu D, Ye T, Wang Z, Cai J, Liu M. 2017. Precambrian continental crust evolution of Hainan Island in South China: Constraints from detrital zircon Hf isotopes of metaclastic-sedimentary rocks in the Shilu Fe-Co-Cu ore district. Precambrian Res, 296: 195–207

(Responsible editor: Huayong CHEN)